



# Temperature-dependent shear localisation and microstructural evolution in machining of nickel-base superalloys



Andrea Ia Monaca<sup>a</sup>, Dragos A. Axinte<sup>a,\*</sup>, Zhirong Liao<sup>a</sup>, Rachid M'Saoubi<sup>b</sup>, Mark C. Hardy<sup>c</sup>

<sup>a</sup>Rolls-Royce UTC in Manufacturing and On-Wing Technology, University of Nottingham, Nottingham NG8 1BB, United Kingdom

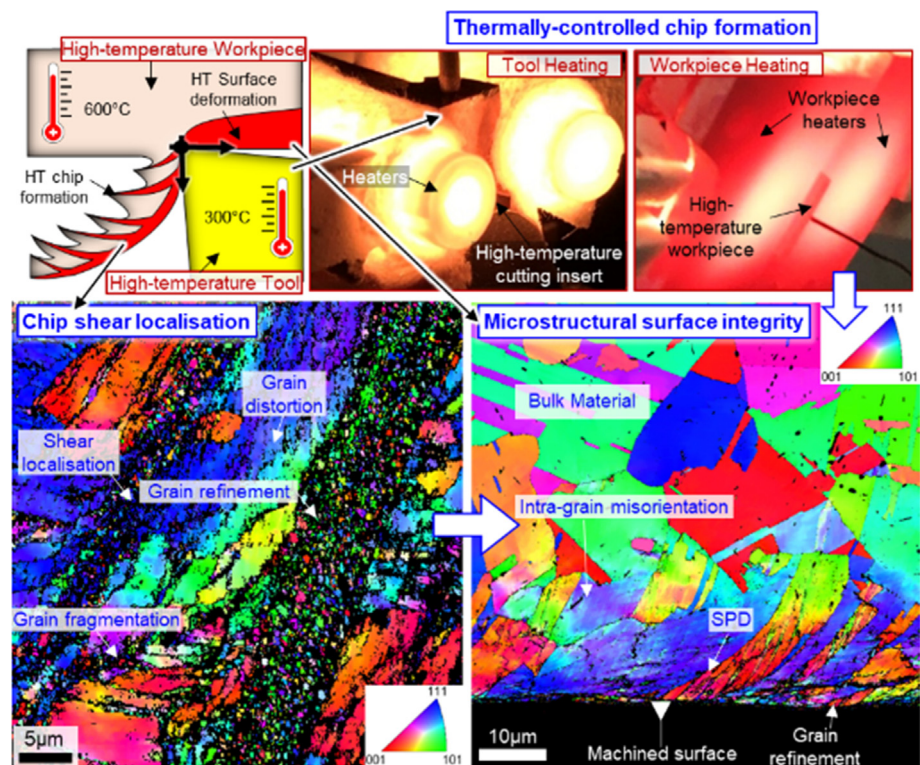
<sup>b</sup>R&D Material and Technology Development, Seco Tools AB, 737 82 Fagersta, Sweden

<sup>c</sup>Rolls-Royce plc, PO Box 31, Derby DE24 8BJ, United Kingdom

## HIGHLIGHTS

- Development of an experimental set-up for investigation of the mechanisms of microstructural surface deformation in machining of Ni superalloys under controlled tool and workpiece temperatures.
- The relationship between cutting energy and microstructural deformation in machining is found to be temperature-dependent.
- Chip serration, shear localisation and grain refinement can be induced individually by increased thermal fields or increased mechanical interaction, with distinction of the role of thermal and mechanical effects.

## GRAPHICAL ABSTRACT



## ARTICLE INFO

### Article history:

Received 7 April 2022

Revised 18 May 2022

Accepted 26 May 2022

Available online 29 May 2022

## ABSTRACT

Understanding the microstructural evolution mechanisms in machining of advanced materials is essential to achieve excellent surface integrity levels within the manufacture of safety-critical components. However, as thermal and mechanical effects are coupled in conventional cutting operations, it is difficult to attribute their individual role on microstructural evolution and integrity. To investigate the temperature-dependency of microstructural evolution in cutting, a new experimental set-up has been

\* Corresponding author.

E-mail address: [Dragos.Axinte@nottingham.ac.uk](mailto:Dragos.Axinte@nottingham.ac.uk) (D.A. Axinte).

---

**Keywords:**

Surface integrity  
Nickel-base superalloys  
Cutting temperature  
Machining  
Grain refinement  
Microstructural evolution

developed to perform machining experiments under controlled temperatures. Results show that an onset in chip shear localisation with nanocrystalline grain refinement can be induced uniquely by an increase in cutting temperature under fixed cutting parameters, which microstructurally controls the transition from continuous to serrated chip formation. Increase in mechanical effects at HT leads to the formation of a continuous chip grain refinement layer, associated to a change in energy partition at the tool-workpiece interface. These small-scale behaviours are found to control the reduction in cutting forces and energy at higher temperatures, with a decrease of  $\sim 25\text{--}30\%$ . Nevertheless, despite the lower deformation energy, HT cutting induced larger amounts of microstructural deformation because of thermal softening effects, further disclosing the role of thermal effects on the interplay between shear localisation, microstructural evolution and surface integrity.

© 2022 The Authors. Published by Elsevier Ltd. This is an open access article under the CC BY license (<http://creativecommons.org/licenses/by/4.0/>).

## 1. Introduction

Excellent levels of microstructural integrity are required when processing advanced materials for the manufacture of key engineering systems such as aeroengine gas turbine components, high-power-density electric motors for automotive or aerospace applications, or parts for nuclear power systems [1,2]. Due to their outstanding mechanical performance and relatively low thermal conductivity, mechanical machining of heat-resistant superalloys can induce intensive thermo-mechanical fields localised at the interface between the machined surface and the cutting tool. In fact, severe plastic deformation (SPD) can be induced to machined surfaces at very high strain rates (up to  $\sim 10^4\text{--}10^5\text{ s}^{-1}$ ) and high temperatures (up to  $> 10^3\text{ }^\circ\text{C}$ ) [3,4]. This can result in significant microstructure alteration, high levels of intragranular lattice rotation, or even formation of nanocrystalline layers [5,6]. When processing advanced materials for safety-critical applications, minimum levels of surface deformation are required to achieve the desired functional performance [7,8], especially to avoid possible promotion of low-cycle fatigue (LCF) crack initiation at high temperatures [9,10]. It is hence essential to understand the mechanisms by which microstructural deformation takes place when machining advanced materials for high-performance engineering applications such as Ni-base superalloys [4], Ti-base alloys [11], steels [12] or soft-magnetic alloys [13].

In fact, a strong coupling exists between thermal and mechanical fields arising in machining [14], as the heat generated due to friction and plastic deformation can induce high-temperature conditions in the cutting zone, which can in turn affect the constitutive behaviour of the material being processed. In this context, despite the remarkable research efforts investigating the mechanisms of microstructural evolution in machining, the current literature is still currently unable to fully disclose what the relationship is between thermal regimes, shear localisation and grain refinement. This is primarily because of the intrinsic lack of control between thermal and mechanical effects in conventional cutting scenarios (e.g. more intensive thermal field through a more aggressive mechanical interaction at the tool workpiece), which makes it difficult to identify in which extent the observed microstructural evolution is thermally or mechanically activated.

High cutting speeds have been identified as a primary parameter responsible for promotion of grain refinement [15], and can determine the onset of different thermal regimes in cutting. In fact, it has been found that dynamic recrystallisation in the chip secondary shear zone (SSZ) can be controlled by a temperature onset causing the transition between cutting regimes and induced layers of equiaxed grains of  $\sim 100\text{ nm}$  size [16]. However, since higher speeds are responsible for an increase in both temperatures and deformation rates, it is difficult to identify the role of thermal and mechanical effects on the grain refinement process. Hosseini et al. [17] have found that dynamic recrystallisation also governed the formation of machining-induced white layers (WLs) under

higher temperatures, whereas dynamic recovery was predominant in WLs induced by prevalent mechanical means. Moreover, Liao et al. [18] have investigated the grain refinement mechanism and nanocrystalline layer formation in advanced Ni-base superalloys, with additional focus on their micromechanical behaviour. However, also in these cases it is still difficult to explain in which extent mechanical and thermal effects are individually accountable for the grain refinement process, as temperature increase was a consequence of the tool-workpiece mechanical interaction. Wang et al. [19] have investigated the role of mechanical effects in high-speed machining of Ti-6Al-4V, showing that chip serration can be highly influenced by presence of stress triaxiality. Nonetheless, it is not known if there is any temperature-dependency of shear localisation and workpiece microstructural deformation. In this context, Liu et al. [20] have studied the dynamic recrystallisation in high speed machining of copper with the development of a numerical model to investigate the role of thermo-mechanical effects on microstructural evolution.

Thermal effects have also been proven to influence the material removal mechanism down to the micro/nano scale when cutting soft/brittle materials [21]. On the other hand, because of differences in thermo-mechanical behaviour this might not be directly applicable to the case of high performance materials e.g. heat-resistant superalloys. Harzallah et al. [22] have investigated the thermo-mechanical coupling existing in orthogonal cutting of Ti-6Al-4V, showing how machining parameters affect thermal and mechanical fields at the tool-workpiece interface, and how this influences chip formation and surface integrity. Similarly, it has been shown the thermo-mechanical history of a machined surface can be related to microstructural evolution and surface integrity in cutting of advanced Ni-base superalloys [23]. Emerging approaches are also considering the influence of microstructural characteristics on machinability and surface integrity when cutting additively-manufactured superalloys [24,25]. However, the thermal fields investigated in these studies are still a consequence of the tool-workpiece mechanical interaction, making it difficult to fully address the temperature-dependency of microstructural reconfiguration.

Although mechanical and thermal effects are generally coupled in machining operations, the process boundary conditions can interfere with their coupling, e.g. in presence of interrupted cutting conditions or when cutting fluids are employed. Nemetz et al. [26] have in fact shown how milling inserts can undergo cyclic heating and cooling conditions during cutting, with focus on the cutting insert's substrate plastic deformation. Nevertheless, it is not known how these thermal boundary conditions could influence the workpiece microstructural evolution. Zhang et al. [27] have reported that highly-refined grain layers can in fact be generated under interrupted cutting conditions for the case of rotary ultrasonic elliptical end milling of Ti-6Al-4V, with grain size below  $100\text{ nm}$ . On the other hand, it is unclear under which thermal conditions microstructural evolution takes place within this discontinuous

cutting process. Presence of wet cutting conditions is also a key factor that can influence the thermal field development in machining. In this context, Cuesta et al. [28] have quantitatively found that in drilling of Alloy 718 the heat being transferred to the workpiece surface could decrease by one order of magnitude in presence of lubricant. In this context, it would be interesting to understand in which way this can affect the machining-induced microstructural evolution.

Approaches have been also developed to artificially increase the material deformation temperature through the additional supply of heat in the cutting zone. In this context, it has been found that through accurate control of the temperature field in laser-assisted milling (LAMill), the surface integrity of Alloy 718 could be improved with respect to conventional milling strategies [29]. Moreover, workpiece pre-heating strategies have been employed to study the influence of cutting temperatures on chip segmentation and microstructural evolution in cutting of Ti-6Al-4V [30], and to investigate thermal softening effects [31] and mechanisms of chip formation in Aluminium alloys [32]. Nonetheless, the role of temperature-dependent shear localisation and grain refinement on the machining-induced microstructural surface integrity has not been considered.

To provide a more general description of the machining-induced microstructural deformation process when cutting advanced alloys, recent studies started to describe this process by means of energy-based approaches [33,34]. In particular, Xu et al. [35] shown that even under different combinations of cutting parameters (such as cutting speeds, tool geometry, wear, etc.) the resulting surface integrity could be linked to the cutting energy dissipated at the tool-workpiece interface. However, the role of different thermal regimes, and their influence on material constitutive response and microstructural evolution is not taken into account.

Thus, a variety of thermal boundary conditions are possible in machining processes and it is not always possible to easily address and interpret the mechanisms of grain refinement in machined surfaces. On one hand, the increase in thermal fields is associated to more aggressive mechanical interaction at the tool-workpiece interface, making it difficult to identify the individual role of thermal and mechanical effects on machining-induced microstructural evolution. On the other hand, the actual thermal field development may be additionally be affected by the process boundary conditions, such as delivery of cutting fluids or performance of interrupted cutting.

Therefore, to understand the temperature-dependency of machining-induced microstructural evolution, the present study investigates the onset of shear localisation and grain refinement when cutting under thermally-controlled conditions. In fact, as outlined in the following sections, the workpiece and the cutting insert are individually heated through external heat sources to perform orthogonal cutting under controlled thermal conditions. This allows identification of the individual role played by thermal and mechanical effects on the microstructural deformation process induced by machining operations to advanced materials.

As a case study, this work applies these concepts to the cutting of Alloy 718 as a representative Ni-base superalloy for high-temperature structural applications, as the mechanisms of machining-induced deformation in these alloys represent an open and active research topic for the materials and manufacturing community.

## 2. Scope of the research

When removing material through chip formation, a system of cutting forces arises at the tool-workpiece interface, which for

orthogonal cutting scenarios has components parallel (Cutting Force,  $F_C$ ) and perpendicular (Thrust Force,  $F_T$ ) to the cutting speed ( $V_C$ ), as shown in Fig. 1a. As reported in [3], under orthogonal cutting conditions, the total cutting energy per unit volume  $u$  can be evaluated as:

$$u = \frac{F_C}{t_0 \cdot w} [J/mm^3] \quad (1)$$

where  $t_0$  represents the uncut chip thickness and  $w$  represents the cutting width. Moreover, the total cutting energy per unit volume  $u$  can also be expressed as sum of the main sources of energy consumption at the tool-workpiece interface [3]. In particular, shear energy ( $u_s$ ) is consumed to induce locally shear workpiece material becoming part of a chip, while friction energy ( $u_f$ ) is dissipated by friction at the interface between the chip and the tool rake, as shown in Fig. 1c. Additionally, when the tool cannot be considered as ideally sharp (e.g. in presence of large tool radii or small depths of cut) the energy consumed due to the ploughing action of the cutting edge on the new workpiece surface is not negligible (Fig. 1c). For orthogonal cutting operations, the contribution of the ploughing energy per unit volume  $u_p$  can be calculated according to the model proposed by Budak et al. [36]. In the present work, this calculation is undertaken following consolidated literature models, consistently with previous work relating energy consumption and partition to microstructural deformation in cutting [35,37]. In particular, the literature approaches used to calculate shear energy and friction energy are presented in Table 1.

Thus, in absence of relevant tool wear, the total cutting energy per unit volume can be expressed as the sum of shear, friction and ploughing energy contributions:

$$u = u_s + u_f + u_p [J/mm^3] \quad (2)$$

In this way, the present work aims to provide a framework to study the mechanisms of shear localisation in machining under controlled thermal conditions. In fact, let us at first consider an orthogonal cutting operation under a fixed set of cutting parameters (cutting speed, feed, width, insert geometry, etc.), where no external heat sources are applied, as in Fig. 1a. During cutting, the energy is consumed at the tool-workpiece interface as microstructural evolution and shear localisation occur within in the chip volume - especially in between chip segments and on its back sliding on the tool rake - and within the new workpiece surface.

For this set of cutting conditions, the resulting surface integrity could be assessed and interpreted by analysis of the energy consumed at the tool-workpiece interface and to the thermo-mechanical effects in the cutting zone. However, the workpiece deformation mechanism is likely to be temperature-dependent. To study the effect of higher cutting temperatures, the tool-workpiece mechanical interaction could be increased, e.g. by imposing higher cutting speeds or feeds. However, the resulting microstructural reconfiguration would be a consequence of an increase in both thermal and mechanical effects, making it difficult to understand their contribution on the resulting microstructural reconfiguration.

As such, what would be instead the individual effect of higher cutting temperatures on chip formation, shear localisation, energy consumption and grain refinement for the same cutting parameters?

To study this problem, higher thermal regimes can be achieved by means of an external heat sources, allowing the performance of the same cutting operations but at higher temperatures (Fig. 1b). On one hand, increasing temperatures might promote localised thermal softening in the chip volume, with increasing amounts of shear localisation and a more intensive microstructural reconfig-

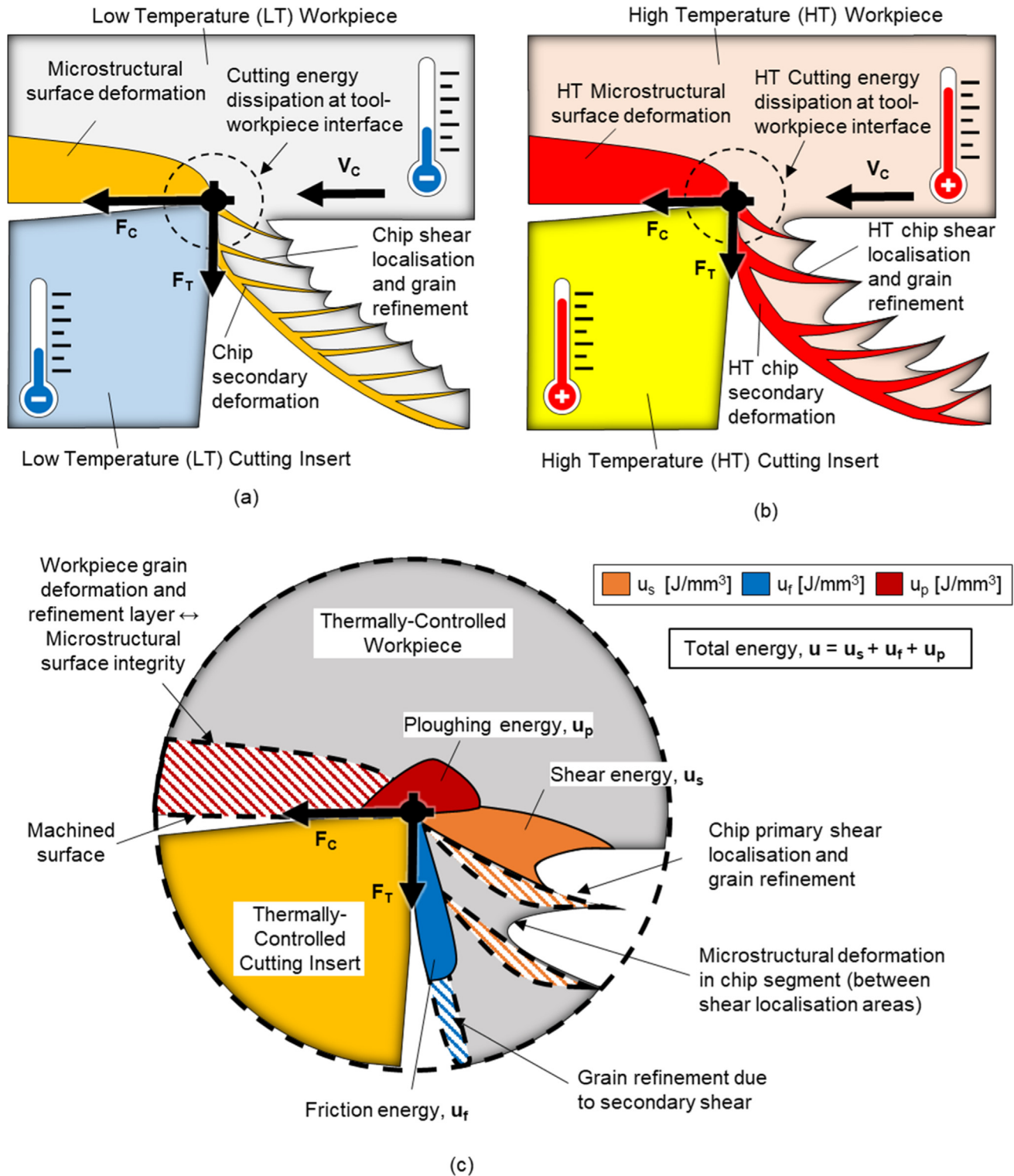


Fig. 1. Chip formation, energy partition, shear localisation and microstructural deformation at the tool-workpiece interface under controlled temperatures. (a) Chip formation mechanisms at low thermal conditions; (b) Chip formation at high thermal conditions. (c) Detail of energy partition and shear localisation at the tool-workpiece interface.

Table 1  
Approaches followed for specific cutting energy calculations and literature references.

Energy contribution	Symbol	Literature model
Shear energy	$u_s$	M.C. Shaw [3]
Friction energy	$u_f$	M.C. Shaw [3]
Ploughing energy	$u_p$	Budak et al. [36]

uration. Macroscopically, this could result in different degrees of chip serration, which would in turn influence the magnitude of the cutting forces exchanged at the tool-workpiece interface and decrease the energy consumption. However, lower cutting energies might not necessarily result in a better surface integrity, as thermal softening in the machined surface could decrease the amount of energy required to impart microstructural deformation.

Thus, in the present research a purposely-designed experimental set-up is employed to perform cutting operations under controlled thermal conditions. The investigation of these phenomena is then applied to a case study considering a reference Ni-base superalloy (Alloy 718). In fact, Ni-base superalloys represent a class of materials for whom their temperature-dependent material response is accounted for most of the complexity during machining operations. Moreover, these materials are employed for the manufacture of safety-critical components requiring excellent levels of microstructural integrity after material removal processes. Hence, this represents a relevant case study to understand the temperature-dependent mechanisms of microstructural evolution during mechanical machining.

### 3. Thermally-controlled orthogonal cutting experiments: Experimental details

#### 3.1. The heat-assisted pendulum-based set-up

In recent years, an effective approach to investigate the machinability and surface integrity of advanced alloys has been developed by adoption of a pendulum-based experimental set-up allowing to efficiently perform orthogonal cutting experiments at room temperature [35]. Within the present research, a pendulum-based cutting machine is equipped with two heating systems controlling the workpiece and cutting insert temperature to investigate the influence of different thermal regimes on chip formation and microstructural reconfiguration during cutting. In particular, a modified Charpy pendulum is employed to perform orthogonal cutting experiments, where a small rectangular sample (1 mm cutting width  $\times$  10 mm cutting length) overhangs from the moving hammer of the pendulum, and a cutting tool is fixed on its stationary base (Fig. 3). Once the pendulum's arm is released, the moving workpiece starts its descent until it engages with the fixed cutting insert leading to chip formation under orthogonal cutting conditions. During this process, cutting forces are recorded through a dynamometer (Kistler 9275B) and cutting speeds are derived by motion tracking through high-speed imaging (recording at 4.5 kHz with an IDT Y4 camera), as shown in Fig. 3 and Fig. 4.

Thus, this allows to observe the chip formation mechanism, evaluate cutting energy partitions, and link this to the microstructural deformation occurring in the workpiece. However, since the

time-in-cut for a 10 mm length is very short (in the range of  $10^{-3}$  s), previous approaches employing pendulum-based cutting strategies without external heat supply were unable to account for the influence of thermal fields on the chip formation mechanism.

To overcome this, two PID-controlled heating systems have been designed to independently heat-up workpiece and the cutting insert to different target temperatures, allowing the performance of orthogonal cutting experiments under controlled thermal conditions (Fig. 3 and Fig. 4). In particular, two ceramic heating elements (Rauschert GmbH) operating at temperatures up to 1100 °C under a PID-modulated 90 V voltage conduct heat by contact with the side faces of the cutting insert, while an N-type thermocouple on the tool flank (Fig. 5b) provides temperature feed-back to the PID controller. Workpiece heating is instead realised by encapsulating 4 ceramic heating elements into two stainless steel bodies in contact with the sample before and during the cutting test (Fig. 3 and Fig. 5c). Specifically, the workpiece heaters are located at a distance of  $\sim$  1 mm from the machined surface, whose temperature is PID-controlled by means of an N-type temperature feed-back (as in Fig. 3 and Fig. 5c). Therefore, as shown in Fig. 5a, this strategy allows to heat-up the machined workpiece and the cutting insert to desired temperatures levels. Once the desired temperatures are reached, the pendulum's arm is released without further set-up time, as the heating systems are designed to stay in place during the whole duration of the cutting process. In this way, the controlled thermal conditions allow to investigate the microstructural evolution, strain localisation and energy partition in machining under different thermal and mechanical regimes for a reference Ni-base superalloy (Alloy 718), as outlined in the next section.

#### 3.2. Cutting scenarios and material analysis

In order to investigate the temperature-dependency of shear localisation and grain refinement in machining of heat-resistant superalloys, the workpiece selected for the present analysis is Alloy 718. The 'as received' Alloy 718 microstructure is presented in Fig. 2 by a representative Inverse Pole Figure (IPF) map obtained through Electron Back-scatter Diffraction (EBSD) analysis. The microstructure of this material consists of a relatively coarse grain size of the gamma matrix (average grain size ASTM 9 to 8), with presence of delta phase particles and carbide precipitates. Alloy 718 is in fact a well-studied Ni-base superalloy often considered as a reference for this class of materials. In terms of high-temperature behaviour, wrought Alloy 718 can have a drop of 15–20% in yield or ultimate tensile strength (UTS) when comparing room temperature (RT) tensile response to 650 °C conditions (where it can still provide UTS of  $\sim$  1000 MPa), as reported in [38].

Thus, as outlined in Table 2, the temperature-dependency of shear localisation and microstructural deformation in this material has been studied for different combinations of thermal and mechanical effects. Specifically, tests #1 and #2 (Table 2) are performed in a lower cutting speed range of  $V_C = 50$  m/min, and with a cutting insert (geometry LCGN160400) having a flat rake and a sharp edge radius ( $\alpha = 0^\circ$ ,  $r = 25 \mu\text{m}$  - PVD coated carbide), at a depth of cut  $t_0 = 0.1$  mm. To understand the influence of temperature on the machining-induced deformation mechanism, this cutting configuration has been tested under two different thermal regimes, i.e., at room temperature (RT) (case #1, Table 2), and at high temperature (HT) with  $T_W = 600$  °C and  $T_T = 300$  °C (case #2, Table 2), to observe the influence of higher thermal effects on the machining-induced microstructural evolution, whilst ensuring that the Alloy 718 workpiece retains sufficient overall strength away from the cutting zone.

Moreover, two additional experiments are considered to investigate the temperature-dependency in machining-induced microstructural evolution under higher material removal rates

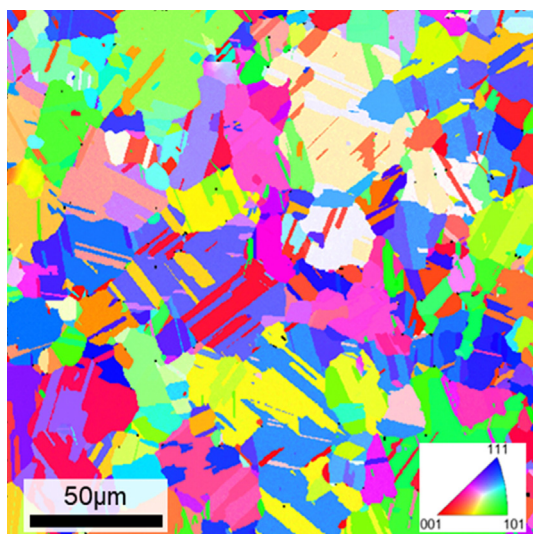
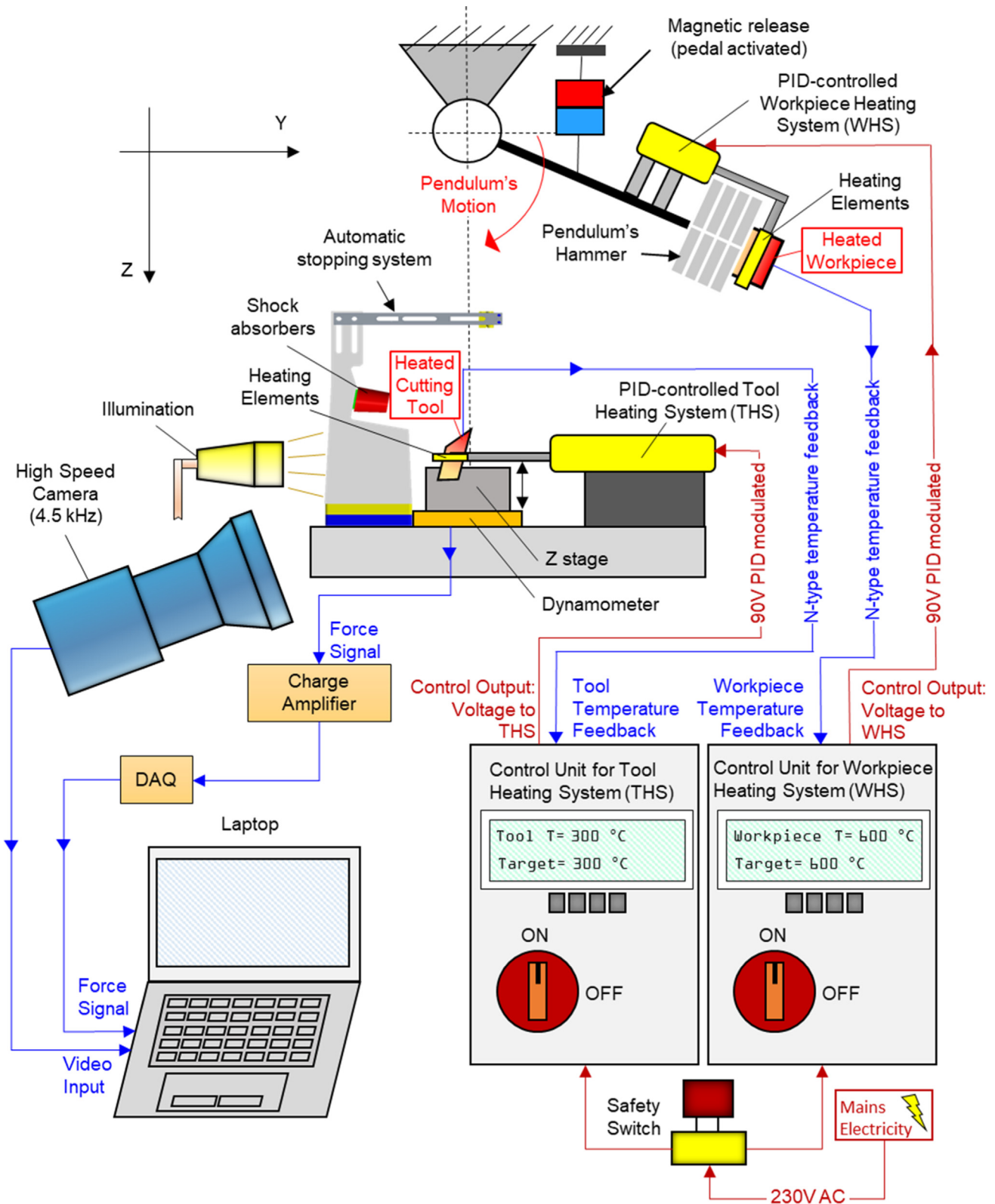


Fig. 2. Electron-backscatter diffraction (EBSD) map displaying the microstructure of the selected Ni-base superalloy 718.



**Fig. 3.** Schematic representation of the heat-assisted pendulum-based cutting test. The target workpiece is placed in the moving hammer of the pendulum while the tool is fixed on its base. High-speed imaging and force signals are acquired in order to derive cutting speeds, power and energies. PID controlled heating systems are applied to the workpiece and to the tool to perform cutting operations under controlled temperatures.

associated to greater mechanical effects. In particular, higher ploughing effects, higher deformation rates and frictional interaction are achieved in experiments #3 and #4 (Table 2) by means

of a higher cutting speed of  $V_c = 140$  m/min and a more frictional insert geometry with negative rake and a greater edge radius ( $\alpha = -10^\circ$ ,  $r = 50 \mu\text{m}$  – PVD coated carbide). In this way, microstructural

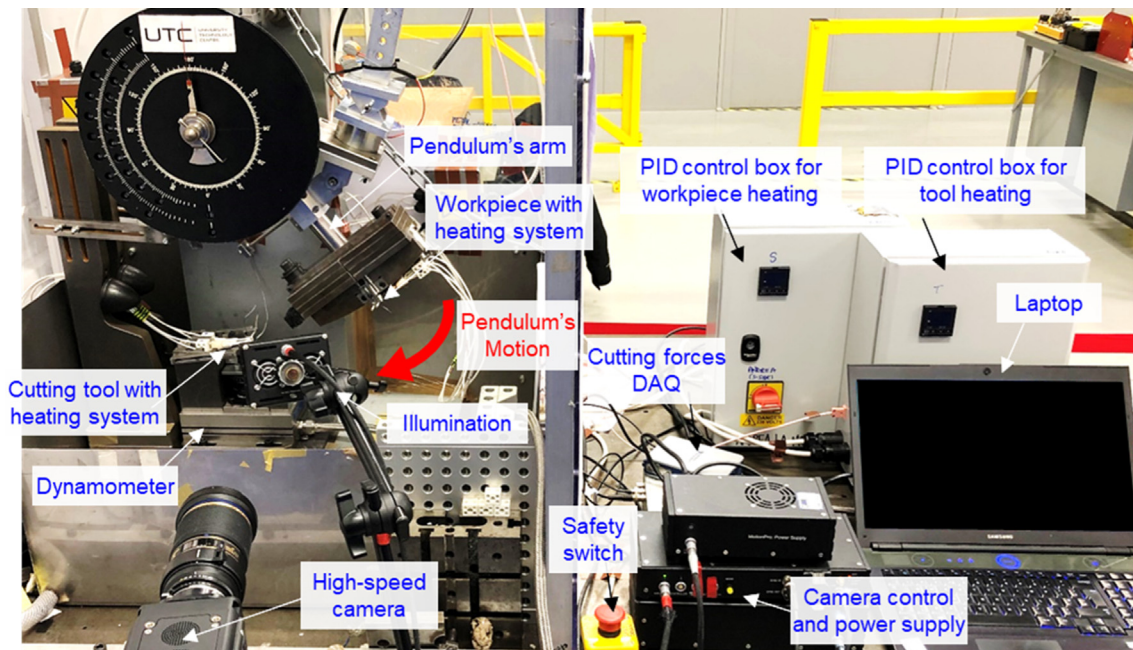


**Fig. 4.** Overall view of the experimental set-up, including: pendulum-based machine, release and stopping system, dynamometer, high-speed camera, illumination, PID controlled heating systems for workpiece and cutting tool, data acquisition systems and laptop. Once the workpiece and the tool are heated up to controlled temperatures, the pendulum's arm is released, chip formation is performed, with high speed video recording and cutting forces acquisition.

evolution induced by aggressive cutting is studied both at low (RT, case #3) and high temperatures ( $T_W = 600$  °C,  $T_T = 300$  °C – case #4).

For each of the cutting scenarios in Table 2, material analysis techniques are applied to investigate presence of shear localisation, microstructural surface deformation and grain refinement in the machined surface and chips, with representative material deformation values obtained as an average from multiple sites within the desired cutting speed range for each specimen (tolerance of  $\pm 1$  m/min). To this aim, the metal samples have been embedded in conductive resin, ground and mirror polished for electron microscopy analysis. Chip morphology observations are carried out through a JEOL7000F field emission gun scanning electron microscope (FEG-SEM), whilst a focused ion beam (FIB) machine (FEI Quanta200 3D FIB-SEM) is employed to observe the levels of microstructural deformation by means of ion channelling contrast (ICC). Furthermore, to disclose full detail on the grain refinement process induced in the machined surfaces and in the chip shear localisation areas, Electron Backscatter Diffraction (EBSD) mapping is employed by means of a Nordlys Max 3 detector (Oxford Instruments) installed on a JEOL7100F FEG-SEM, with step sizes smaller than 100 nm. The resulting crystallographic map data are presented in 'as-detected' form without application of any noise-reduction or smoothing strategies. In this way, the influence of temperature on the chip formation mechanism, shear localisation, cutting energy consumption and machining-induced microstructural evolution can be investigated and disclosed with application to the case of Ni-base superalloy 718.

## 4. Results and discussion

### 4.1. The macroscopic role of temperature-dependent effects on chip formation: Analysis of cutting forces, energy partition and chip morphology

To understand the physical conditions under which small-scale microstructural deformation and grain refinement take place at the

tool-chip and tool-workpiece interface, the cutting experiments outlined in Table 2 are first investigated from a more macroscopic perspective in terms of cutting forces ( $F_T$ ,  $F_C$ ), specific cutting forces ( $K_T$ ,  $K_C$ ), energy consumption and chip morphology.

Within the pendulum-based cutting method, the workpiece experiences a reduction in cutting speed as cutting energy is consumed during chip formation. In the past, this effect has been exploited to analyse multiple speed parameters within a single specimen and continuously map their influence on surface integrity [35,37]. In fact, high-speed imaging combined with motion tracking allows to continuously evaluate the cutting speed at each workpiece location between the tool entry and exit sections. In this work, this approach was employed to identify regions of the workpiece where chip formation took place at the desired speed range for subsequent surface integrity analysis. Specifically, combining speed profiles in Fig. 6(a) with the corresponding force profiles in Fig. 6(b,c) allowed to identify cutting data at each workpiece location, and in particular in the sites of interest within the experimental scenarios defined in Table 2.

Starting from the analysis of the experiments performed in the low speed range ( $V_C = 50$  m/min,  $\alpha = 0^\circ$ ,  $r = 25$   $\mu$ m), a  $\sim 25\%$  drop in cutting forces (Fig. 7a) and specific cutting energy (Fig. 7b) is observed when increasing the cutting temperature, i.e. when moving from *low-speed/low-temperature* conditions (RT, case #1) to *low-speed/high-temperature* ( $T_W = 600$  °C,  $T_T = 300$  °C – case #2). All the individual energy contributions attributed to shear, friction and ploughing effects decrease at higher temperatures (Fig. 7c), but without a significant change in relative weight to the total cutting energy (Fig. 7d).

On one hand, lower forces and cutting energy at higher temperatures can be associated to a decrease in the alloy's strength compared to RT conditions. However, this can also occur due to a change in chip formation, as its shear localisation mechanism can be affected by an increase in deformation temperature. In fact, SEM examination reveals that greater chip serration is induced at higher temperatures, i.e. at *low-speed/high-temperature* conditions (Fig. 8b – case #2) compared to *low-speed/low temperature*

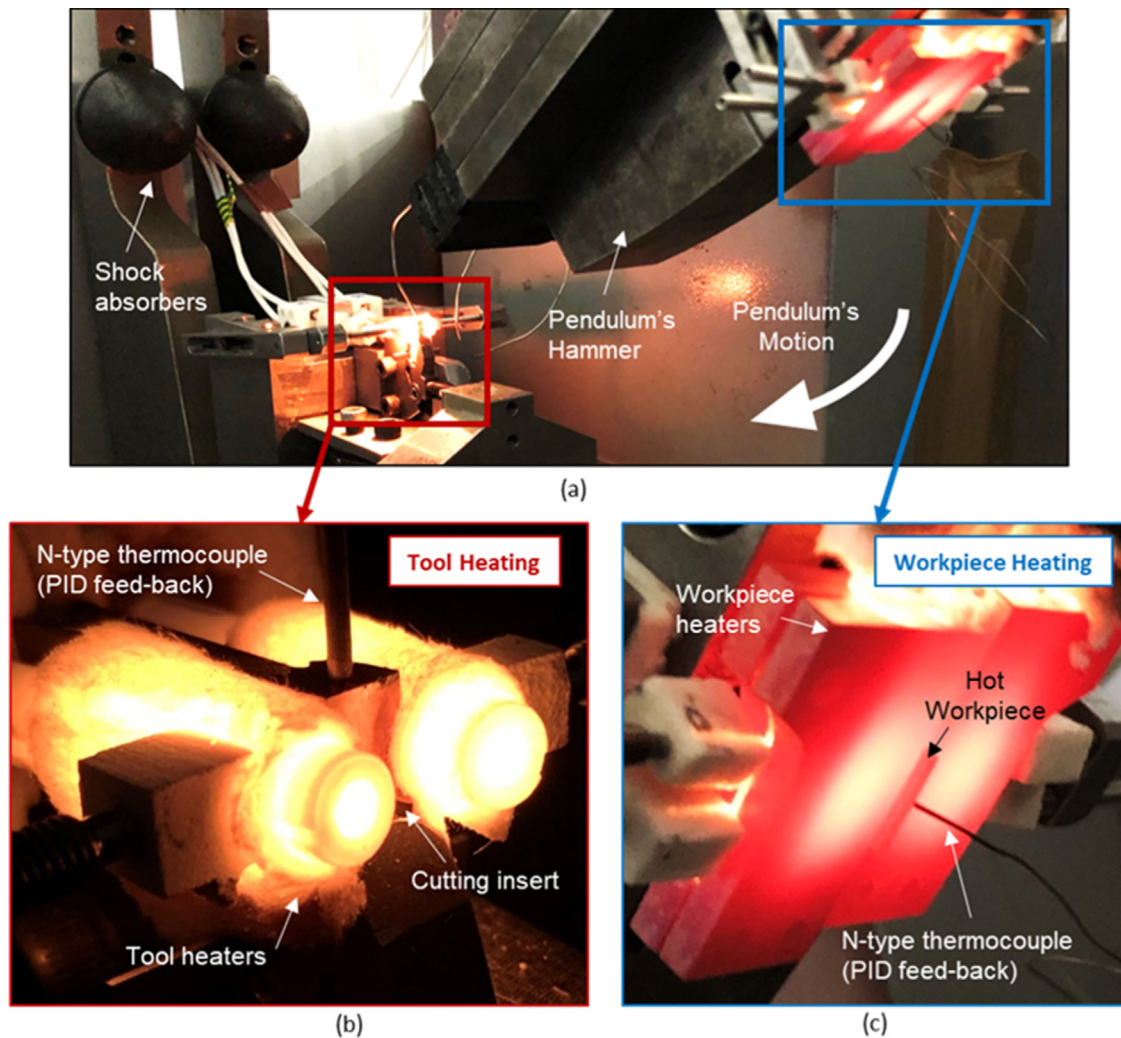


**Fig. 5.** High-temperature cutting configuration. (a) Pendulum set-up with operating heating system both on the tool and on the workpiece. (b) Detail view of the tool heating system and feed-back temperature measurement on the rake face. (c) Detail view of workpiece heating system and feed-back temperature measurement.

**Table 2**

Experimental orthogonal cutting conditions considered to reveal the influence of different thermal regimes on microstructural evolution under lower and higher mechanical effects. Cutting width ( $w$ ) and uncut chip thickness ( $t_0$ ) are the same in all tests and equal to 1 mm and 0.1 mm, respectively. Same PVD coated cemented carbide cutting tool grade (Seco Tools) is used for all tests.

Case #	Mechanical Effect	Thermal Effect	$T_w$ [°C]	$T_r$ [°C]
1	Low Mechanical Effect	Low	RT	RT
2	$V_c = 50$ m/min; $\alpha = 0^\circ$ ; $r = 25$ $\mu$ m;	High	600	300
3	High Mechanical Effect	Low	RT	RT
4	$V_c = 140$ m/min; $\alpha = -10^\circ$ ; $r = 50$ $\mu$ m;	High	600	300

(Fig. 8a - case #1). This relates to the high-temperature decrease in shear and friction energy (Fig. 9a), which together with a higher chip serration degree  $\zeta$  (Fig. 9b) indicates an increase in chip shear localisation.

Thus, the preliminary macroscopic analysis of chip formation under low mechanical effects shows that an increase in thermal field can produce a decrease in cutting forces due to an interplay between a lower material response and a shift in chip formation mechanisms towards increased serration degrees.

Also when considering chip formation within the *high-speed* range ( $V_c = 140$  m/min,  $\alpha = -10^\circ$ ,  $r = 50$   $\mu$ m), lower cutting forces (Fig. 7a) and lower energy consumption (Fig. 7b) is observed at

higher temperatures, i.e. *high-speed/high-temperature* (case #4) compared to the *high-speed/low-temperature* configuration (case #3), with an average decrease in the range of  $\sim 28$ – $30\%$ . However, under such more aggressive mechanical interaction, tool-chip friction represents the main source of energy consumption (Fig. 7c) in both thermal ranges, i.e. at *high-speed/low-temperature* (case #3) and at *high-speed/high-temperature* (case #4), differently from the low-speed experiments (cases #1 and #2) where shear energy consumption was predominant (cases #1 and #2). Specifically, the observed increase in friction and ploughing energy is a consequence of the larger tool radius and negative rake angle adopted in cases #3 and #4 (Fig. 7c), as well as the higher cutting speed.

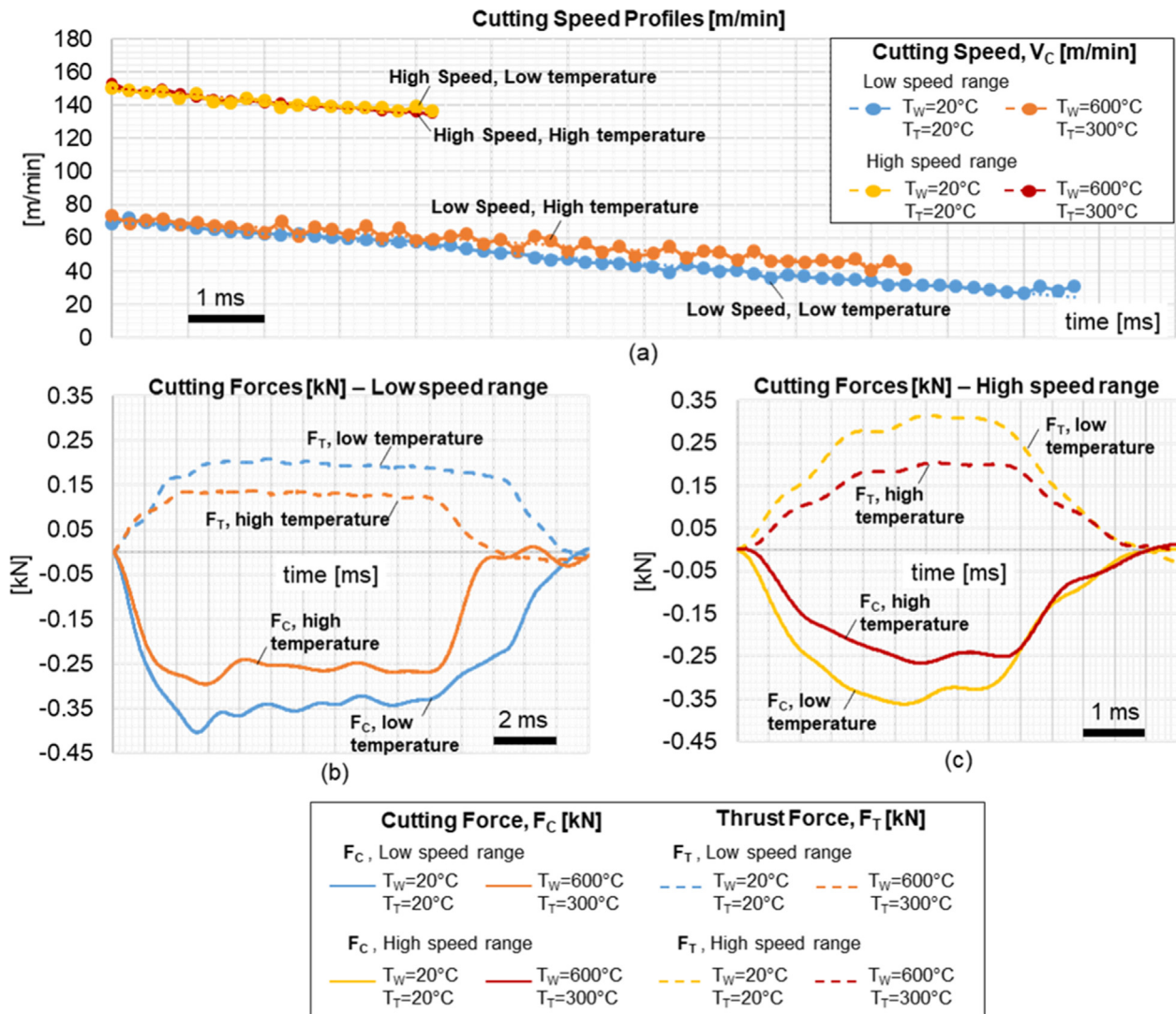


**Fig. 6.** Cutting speeds and forces profiles under different thermal and mechanical conditions during pendulum cutting. (a) Cutting speed profiles. (b) Cutting forces profiles for machining experiments in the lower speed range at low and high temperatures. (c) Cutting forces profiles for machining experiments in the higher speed range at low and high temperatures.

When it comes to the decrease in shear energy (Fig. 9a), this is mainly attributed to the higher cutting speed promoting more intensive shear localisation at higher strain rates, which is further indicated by the more serrated chip morphology (Fig. 8) with higher serration degrees (Fig. 9b). Finally, also within the higher speed range an increase in temperature is responsible for a transition in chip formation mechanism towards higher levels of serration (comparing Fig. 8c with Fig. 8d) as quantitatively confirmed by the plots in Fig. 9d reporting greater serration degrees at HT (case #4) compared to RT (case #3).

Hence, the chip formation mechanisms is affected by both mechanical and thermal effects. As shown in Fig. 8, higher chip serration with more localised deformation was induced by an increase in cutting temperatures at the same cutting speed. Moreover, higher deformation rates at higher speed are also responsible for more serrated chips, with almost separated chip segments for the case combining highest thermal and mechanical effects (Fig. 8d).

Higher temperatures also induced a general decrease in cutting energies and forces at the tool-workpiece interface. In the past, a decrease in cutting energy consumption has been mainly associated with a better surface integrity, i.e. to a lower extent of plastic deformation in the machined subsurface, but without considering

temperature-dependent scenarios. However, this paradigm might no longer be valid when considering the role of different deformation temperatures, as they might affect both the material constitutive response and the chip formation mechanism.

Thus, the interplay between thermal regime, shear localisation, chip formation and microstructural surface integrity is investigated in the following sections, with focus on how the workpiece microstructural reconfiguration takes place as a result of changes in thermal regime, tool-workpiece mechanical interaction and chip serration mechanism.

#### 4.2. Microstructural surface integrity under different thermo-mechanical conditions

As a result of the thermo-mechanical conditions under which the workpiece material deforms at the tool-workpiece interface, significant levels of microstructural alteration and grain refinement can be induced near the newly machined surface. In order to characterise the extent of the machining-induced deformation layers, the machined surfaces have been observed in cross section (parallel to the cutting direction) for each of the experimental scenarios. In this section, the analysis first focuses on the thickness of

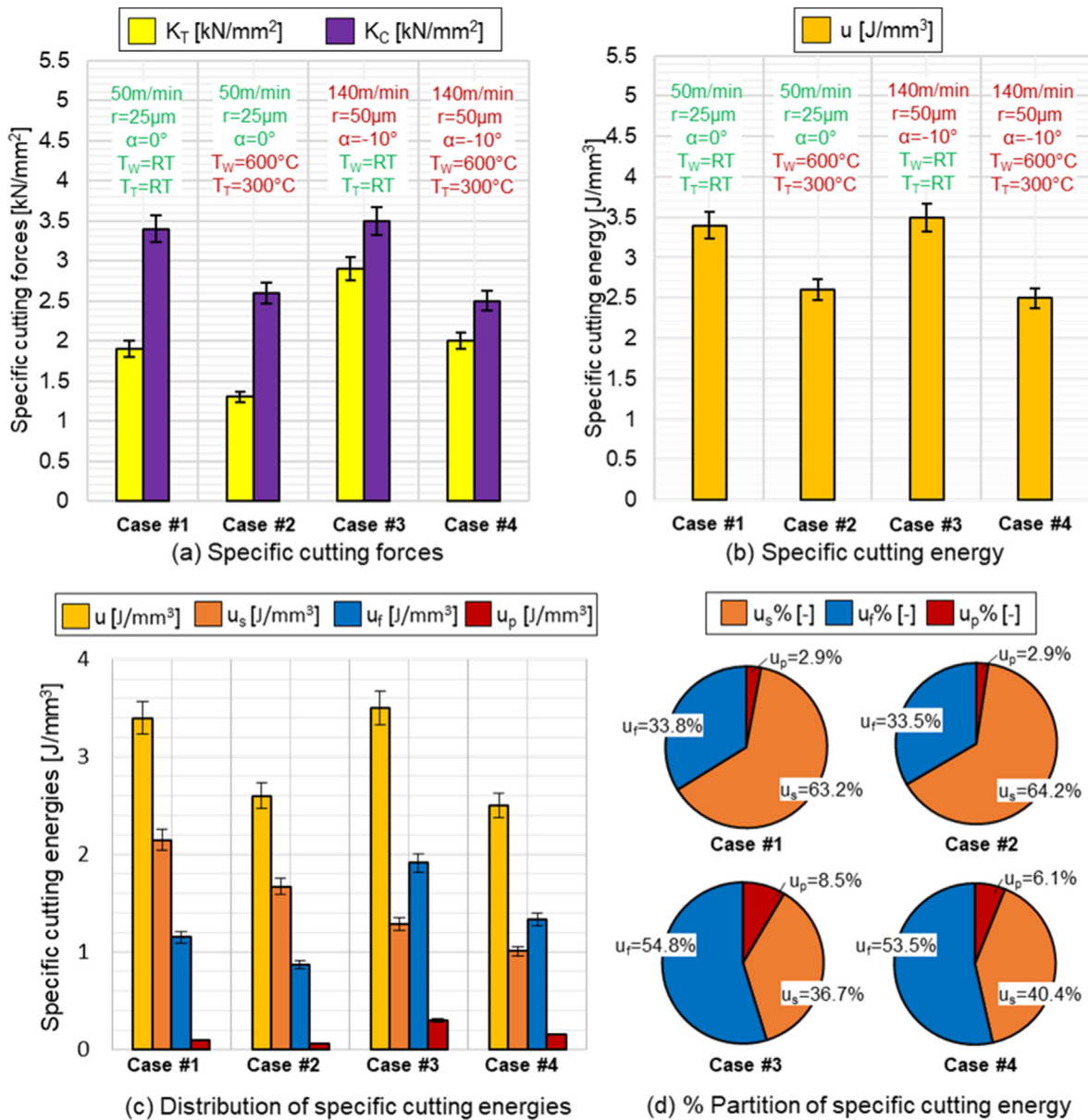


**Fig. 7.** Influence of different thermo-mechanical conditions on specific cutting forces, energy and energy partition. (a) Specific forces during chip formation ( $K_C$  - specific cutting force,  $K_T$  - specific thrust force) and (b) specific cutting energy. (c) Specific energy components and (d) energy partitions.

the machining-induced deformation layers as observed through ion contrast channelling (ICC) to reveal presence of microstructural distortion, before moving to a more in-depth crystallographic analysis through EBSD orientation mapping.

In fact, understanding up to which subsurface depth material deformation occurs is of primary interest as this property of machined surfaces has been linked to their functional performance under high-temperature fatigue loading conditions [8,39]. In the past, it has been observed how the thickness of the deformed layer could be related to the amount of cutting energy dissipated at the tool-workpiece interface [35]. However, previous works have only focused on relatively similar thermal boundary conditions, hence being unable to account for temperature-dependent effects on the microstructural deformation process.

As shown by the ion channelling contrast (ICC) micrograph in Fig. 10a, when cutting under low mechanical effects ( $V_c = 50$  m/min,  $\alpha = 0^\circ$ ,  $r = 25 \mu\text{m}$ ) at room temperature, i.e. *low-speed/low-*

*temperature* (RT – case #1), presence of microstructural deformation is predominant in material regions near the machined surface, gradually decreasing towards the bulk material. Specifically, grain fragmentation and refinement is observed in the near-surface region (Fig. 10b) as a result of the tool-workpiece interaction, with presence of microstructural deformation up to a subsurface depth of  $\sim 30 \mu\text{m}$  (Fig. 11b), corresponding to a ploughing energy level of  $\sim 0.1 \text{ J/mm}^3$  (Fig. 11a).

From a surface integrity perspective, what would be the effect of higher thermal fields for the same set of cutting parameters? Let us now consider the subsurface deformation induced by the same cutting condition ( $V_c = 50$  m/min,  $\alpha = 0^\circ$ ,  $r = 25 \mu\text{m}$ ) but at high temperatures, i.e. *low-speed/high-temperature* ( $T_w = 600^\circ\text{C}$ ,  $T_T = 300^\circ\text{C}$  – case #2). Although higher thermal effects induced lower cutting forces and lower ploughing energy ( $\sim 0.06 \text{ J/mm}^3$ , Fig. 11a), the workpiece material still presents a significant amount of microstructural distortion (Fig. 10c) up to a subsurface depth

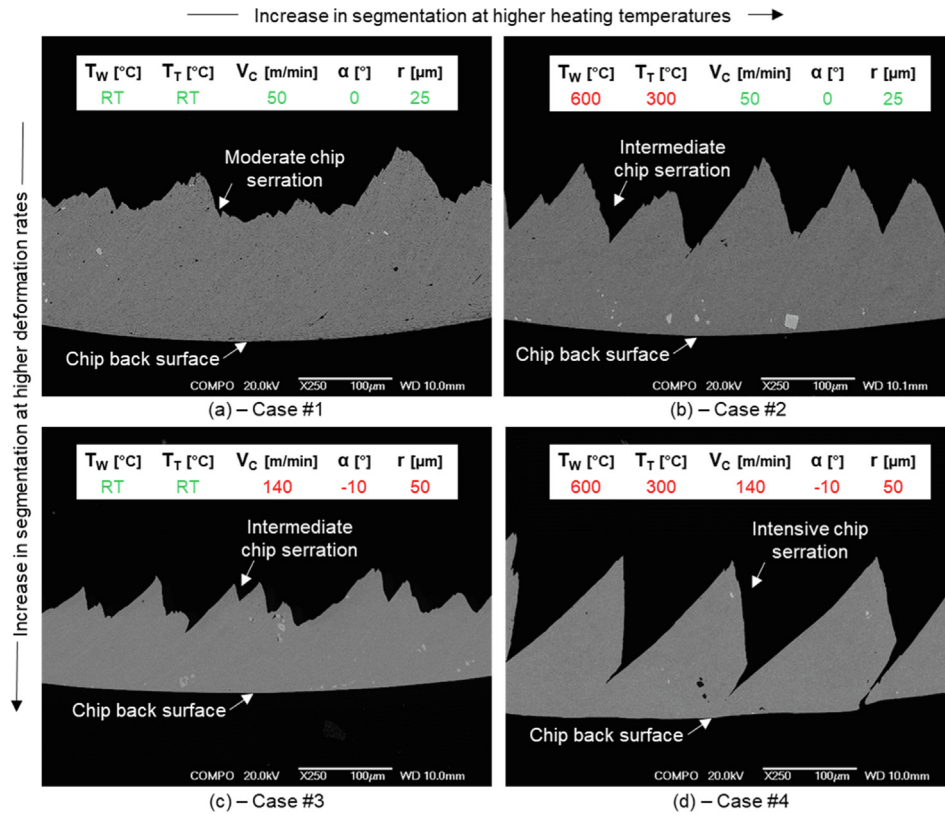


**Fig. 8.** Chip morphology affected by different thermal regimes under lower and higher mechanical effects. (a) Moderate chip serration induced by low thermal effects and low mechanical effects. (b) Intermediate chip serration induced by high thermal effects and low mechanical effects. (c) Intermediate chip serration induced by low thermal effects and high mechanical effects. (d) Intensive chip serration induced by high thermal effects and high mechanical effects.

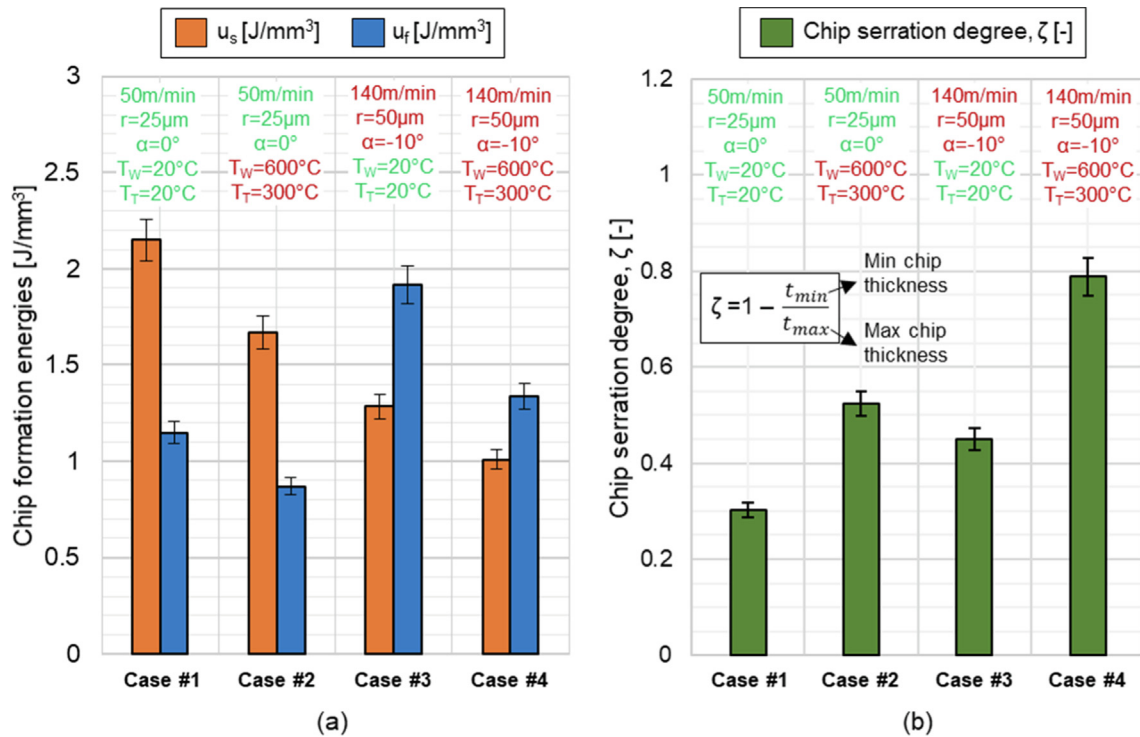


**Fig. 9.** Chip formation energy and serration degrees under different thermo-mechanical conditions. (a) Shear energy and friction energy contributions. (b) Chip serration degrees under different thermo-mechanical conditions.

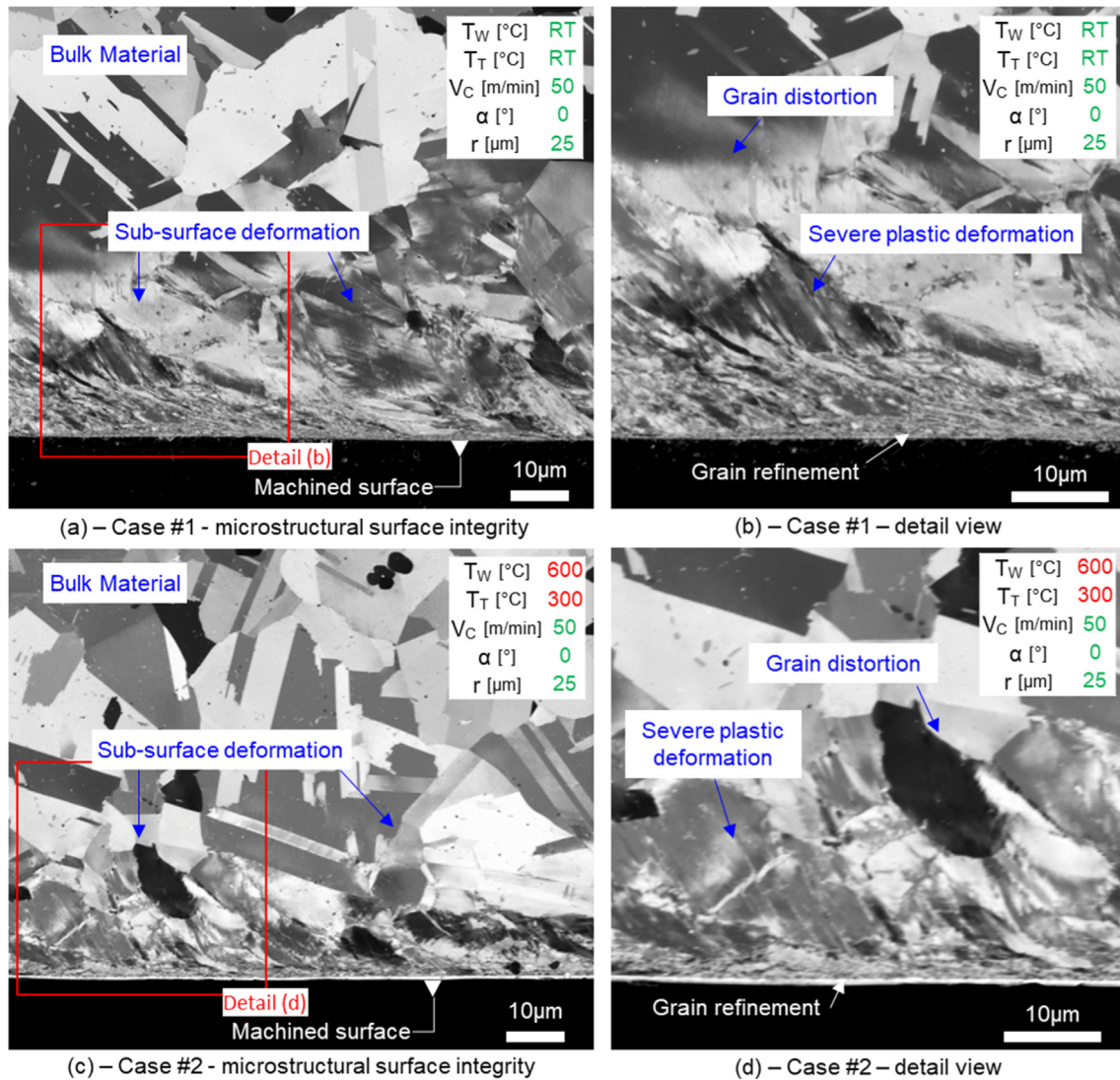


**Fig. 10.** Ion channelling contrast (ICC) analysis of microstructural surface integrity under low mechanical effects. (a) Microstructural deformation under lower thermal effects and (b) near-surface detail. (c) Microstructural deformation under higher thermal effects and (d) near-surface detail.

of  $\sim 33 \mu\text{m}$  (Fig. 11b), with similar indications of severe plastic deformation and grain refinement in regions near the machined surface (Fig. 10d).

Hence, despite the lower cutting forces and lower deformation energy, cutting under higher thermal fields still induced relatively similar (or even higher) extents of subsurface deformation layers compared to the corresponding room temperature condition. Hence, the drop in cutting energy experienced when moving to higher temperature conditions did not correspond to an improvement in the machining-induced microstructural integrity. In fact, when moving towards higher temperatures, less energy is required to produce microstructural deformation, which is in this case attributed to a decrease in yield strength and UTS of wrought Alloy 718 when moving from RT to  $\sim 600 \text{ }^\circ\text{C}$  [38].

A similar tendency is also encountered when considering the machining experiments performed under high mechanical effects ( $V_C = 140 \text{ m/min}$ ,  $\alpha = -10^\circ$ ,  $r = 50 \mu\text{m}$ ), which induced a much more severe deformation in the workpiece microstructure both at *high-speed/low-temperature* (RT - case #3) and *high-speed/high-temperature* ( $T_W = 600 \text{ }^\circ\text{C}$ ,  $T_T = 300 \text{ }^\circ\text{C}$  - case #4). In fact, when aggressively cutting at *high-speed/low-temperature* (RT - case #3), thick deformation layers in the range of  $\sim 45 \mu\text{m}$  extent

(Fig. 11b) are produced, as shown by the micrograph in Fig. 12a. Specifically, extensive presence of severe plastic deformation can be observed in the detail view in Fig. 12c, with a severely-distorted microstructure and formation of highly-refined grain layers in the proximity of the machined surface.

To this microstructural condition (case #3) are associated ploughing energy levels in the range of  $\sim 0.3 \text{ J/mm}^3$  (Fig. 11a), i.e. about three times higher than the corresponding room temperature (RT) experiment under low mechanical effects, i.e. *low-speed/low-temperature* (case #1). Hence, when comparing the two RT conditions, to an increase in deformation energy corresponded an increase in the thickness of the microstructurally-deformed layer.

However, when considering the same aggressive cutting parameters used in case #3 ( $V_C = 140 \text{ m/min}$ ,  $\alpha = -10^\circ$ ,  $r = 50 \mu\text{m}$ ), but at higher temperatures, i.e. under *high-speed/high-temperature* conditions ( $T_W = 600 \text{ }^\circ\text{C}$ ,  $T_T = 300 \text{ }^\circ\text{C}$  - case #4), this resulted in a drop in cutting forces and ploughing energy ( $u_p \sim 0.15 \text{ J/mm}^3$ , Fig. 11a), but actually the severity of the machining-induced microstructural deformation reaches the highest levels ( $>60 \mu\text{m}$  in thickness, Fig. 11b), as shown by the ICC micrograph in Fig. 12b. More in detail, this microstructural state is also characterised by extensive grain sweep, microstructural distortion and submicron grain

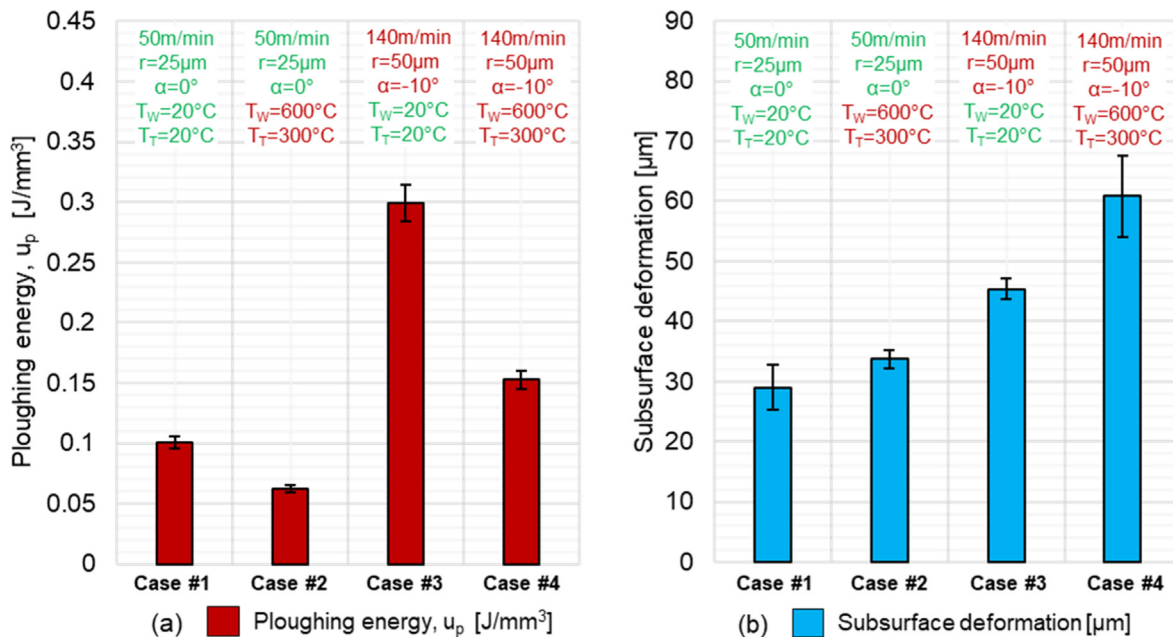


**Fig. 11.** Subsurface deformation and specific ploughing energy under different combinations of thermal and mechanical effects. (a) Ploughing energy under different thermo-mechanical effects. (b) Subsurface deformation extent from Ion channelling contrast analysis.

refinement (Fig. 12d) as a result of the high-temperature deformation process.

Thus, ICC surface integrity analysis has indicated that thermally-controlled effects play a key role on the machining-induced surface deformation. In fact, the thermal regime under which deformation takes place can have an influence on the relationship between cutting energy and microstructural evolution. Specifically, although in similar thermal boundary conditions an increase in specific cutting energy can be used to characterise the resulting surface integrity, this is no longer sufficient when comparing scenarios involving different thermal boundary conditions due to temperature-dependencies in the workpiece material behaviour. To further investigate this tendency, the following sections focus on the effect of the different thermomechanical conditions on the lattice condition and grain refinement observed in the machined surfaces and on the shear localisation process and microstructural evolution induced in the machining chips.

#### 4.3. Temperature-dependent lattice distortion and grain refinement in machined surfaces

In order to further investigate the role of thermal effects on the machining-induced microstructural surface integrity, Electron Backscatter Diffraction (EBSD) has been employed to map the crystallographic condition resulting in the workpiece subsurfaces. In Fig. 13, inverse pole figure (IPF) maps are considered for the experiments involving low mechanical effects, i.e. case #1 at low-speed/low-temperature in Fig. 13a, and case #2 at low-speed/high-temperature in Fig. 13b.

Previous ICC microstructural analysis indicated that higher temperatures induced a decrease in deformation energy, but not in the thickness of the microstructurally-affected layers. In fact, in both thermal ranges under low mechanical effects, i.e. low-speed/low-temperature (Fig. 13a) and low-speed/high-temperature (Fig. 13b) cutting induced significant lattice distortion, with presence of severe plastic deformation, shear localisation and grain refinement predominantly in the areas nearest to the machined surface.

Nevertheless, when moving away from the machined surface towards the bulk material region, although grain sweep and refinement is progressively less evident, the orientation maps in Fig. 13a-b both reveal presence of intra-grain misorientation due to the plastic deformation process. Hence, when moving to higher deformation temperatures under same machining parameters (case #2), a similar crystallographic condition is observed which however corresponded to a  $\sim 40\%$  lower ploughing energy, i.e.  $0.1 \text{ J/mm}^3$  for case #1 at low-speed/low-temperature, compared to  $0.06 \text{ J/mm}^3$  for case #2 at low-speed/high-temperature.

A much more distorted lattice condition is observed under higher mechanical effects both at RT (Fig. 14a,c – case #3) and HT (Fig. 14b,d – case #4). At high-speed/low-temperature (Fig. 14a, c – case #3), presence of grain fragmentation is more significant beneath the machined surface, as shown in detail in Fig. 13c. On the contrary, when moving towards higher temperatures, i.e. at high-speed/high-temperature (Fig. 14b,d – case #4) grain fragmentation is localised in the vicinity of the machined surface, whereas intra-grain deformation is predominant and more extensive towards higher subsurface depths, as shown in the detail view in Fig. 14d.

This behaviour might at first seem to be counter-intuitive, as higher deformation temperatures are in general associated with promotion of grain refinement. However, it can be observed how the higher material ductility at higher temperatures allows the grains to elongate over more extended volumes (as in Fig. 14d), whilst at room temperature (RT) the deformation is constrained at lower subsurface depths (Fig. 14c) thus promoting a more localised deformation process resulting in mechanically-induced grain fragmentation. In terms of intra-grain deformation, additional insights into the crystallographic state induced in the machined subsurfaces is provided by analysis of the Average Intra-grain Misorientation (AMIS).

As reported in previous studies, the AMIS factor can be employed to indicate the relative difference in orientation between crystals belonging to the same grain at each subsurface depth. Thus, AMIS values can be calculated over each line of  $N$  points crossing  $M$  grains with the following equation [40,41], where  $\Theta_{jk}$

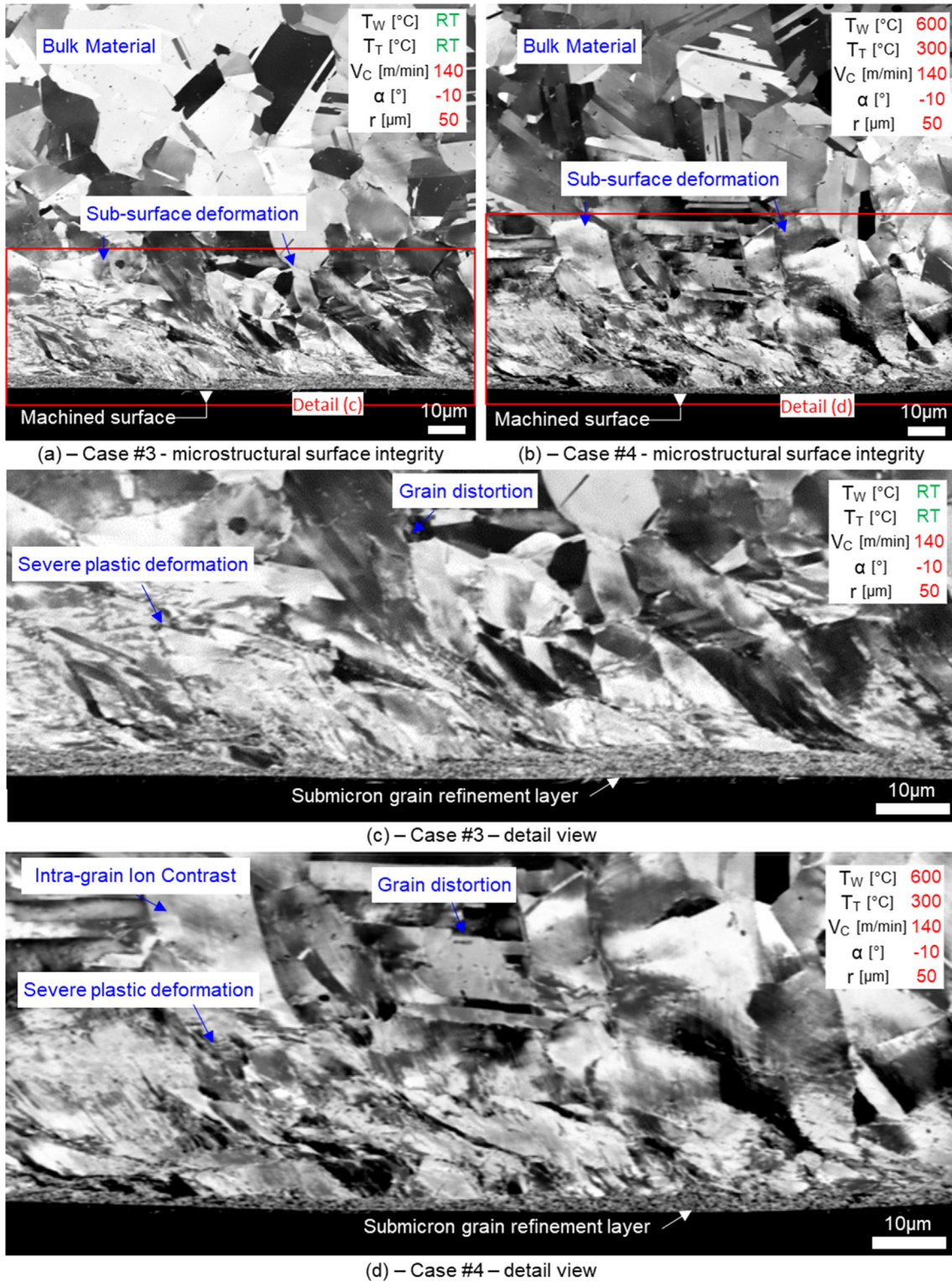


**Fig. 12.** Ion channelling contrast (ICC) analysis of microstructural surface integrity under high mechanical effects. (a) Microstructural deformation under lower thermal effects and (b) near-surface detail. (c) Microstructural deformation under higher thermal effects and (d) near-surface detail.

represents the misorientation angle between each two points  $j$  and  $k$  belonging to the same grain  $i$ :

$$AMIS = \frac{1}{M} \sum_{i=1}^M \left( \frac{2 \sum_{j=2}^N \sum_{k=1}^j \theta_{jk}}{N_i(N_i - 1)} \right)_{\text{grain}(i)} \quad (3)$$

For the case of low mechanical effects, high AMIS values are found in similar subsurface depths at both *low-speed/low-temperature* (case #1) and *low-speed/high-temperature* (case #2), as reported in Fig. 15a. In fact, for both RT and HT conditions higher AMIS levels are found up to a depth of ~ 35 μm.

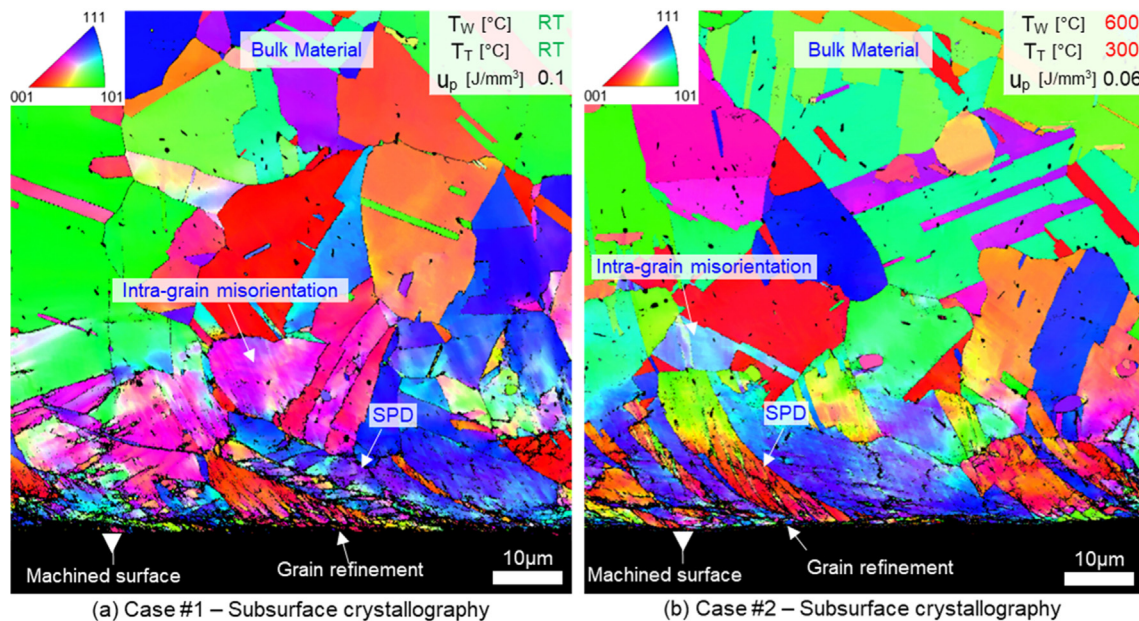


**Fig. 13.** Electron backscatter diffraction (EBSD) analysis of subsurface change in crystallographic orientation under low mechanical effects. (a) Microstructural deformation under lower thermal effects and (b) under higher thermal effects. Despite the decrease in cutting energy at higher temperature, lattice distortion propagates at comparable subsurface depths in both low and high temperature regimes.

Higher mechanical effects are instead responsible for high AMIS levels up to  $\sim 60 \mu\text{m}$  subsurface depths, with similar tendency at both RT (case #3) and HT (case #4), as shown in Fig. 15b. Thus, this further indicates that under high temperature conditions, plastic deformation and lattice anomalies propagated to similar or higher extents beneath the workpiece subsurface, despite the lower deformation energy and lower cutting forces at the tool-workpiece interface.

#### 4.4. Temperature-dependent mechanisms of shear localisation and grain refinement in machined chips

The small-scale shear localisation process governing chip formation has a crucial influence on key macroscopic aspects of machining, such as cutting forces, energy, vibrations as well as surface integrity. Specifically, workpiece volumes are transformed into chips after undergoing severe plastic deformation (SPD) within the so-called “primary shear zone” (PSZ). While in continuous chip formation PSZ can be regarded as a steady-state shear plane [3], serrated chip formation involves unsteady shear localisation in narrow material volumes also referred to as “shear bands”, where material deformation takes place almost instantaneously under adiabatic conditions [42,43].

From a microstructural perspective, chip formation is governed by the mechanism by which its crystals deform and rearrange under the machining-induced thermo-mechanical effects. However, to this point it has been difficult to identify the role of different thermal regimes on the chip microstructural evolution, as within conventional scenarios higher cutting temperatures are associated with a higher mechanical interaction at the tool-workpiece interface. Differently, the present temperature-control strategy allows to investigate the role of different temperatures on the chip microstructural reconfiguration and how this relates to the cutting regime, energy partition and surface integrity. To this aim, the small scale deformation induced in the chips has been investigated from a crystallographic standpoint through electron backscatter diffraction (EBSD) analysis.

Specifically, Fig. 16 shows a chip produced at RT under low mechanical effects ( $V_c = 50 \text{ m/min}$ ,  $\alpha = 0^\circ$ ,  $r = 25 \mu\text{m}$ , RT – case #1), where EBSD indexing has been carried out in the region marked in red in Fig. 16a. As visible in the crystallographic maps in Fig. 16b–e, chip formation at *low-speed/low-temperature* is achieved through a distributed rather than localised plastic deformation process. In fact, presence of grain sweep and elongation is observed throughout the whole chip cross-section, revealing that its grains coherently deformed with limited intensification regions. On greater length scales, this more uniform deformation pattern resulted in a low-serrated/continuous morphology.

Differently, increased thermal effects under *low-speed/high-temperature* conditions ( $T_w = 600 \text{ }^\circ\text{C}$ ,  $T_t = 300 \text{ }^\circ\text{C}$  – case #2) resulted in a significant increase in chip serration, as shown in Fig. 16f, suggesting that higher thermal effects induced an increase in shear localisation. From a crystallographic perspective, EBSD mapping (Fig. 16g–j) reveals that increased serration is achieved through a very heterogeneous deformation pattern within the chip volume, where intensive microstructural reconfiguration is focused in narrow shear bands at the interface between consecutive chip segments that are instead constituted by larger and less deformed grains.

Further insight on the role of temperature on the microstructural evolution governing chip formation is provided by a detail view in the shear localisation areas produced under same cutting parameters ( $V_c = 50 \text{ m/min}$ ,  $\alpha = 0^\circ$ ,  $r = 25 \mu\text{m}$ ) at low (RT – case #1) and high temperature ( $T_w = 600 \text{ }^\circ\text{C}$ ,  $T_t = 300 \text{ }^\circ\text{C}$  – case #2), as shown in Fig. 17.

At low temperature, chip deformation in PSZ predominantly resulted in grain sweep and elongation (Fig. 17a) inducing higher values of intra-granular misorientation especially across larger crystals and at the grain boundaries (Fig. 17b), and with limited occurrence of grain refinement within the micron scale. Differently, when considering the chip produced at higher temperature (Fig. 17c–d), PSZ deformation is much more localised, with formation of narrow shear bands where submicron recrystallisation occurred.

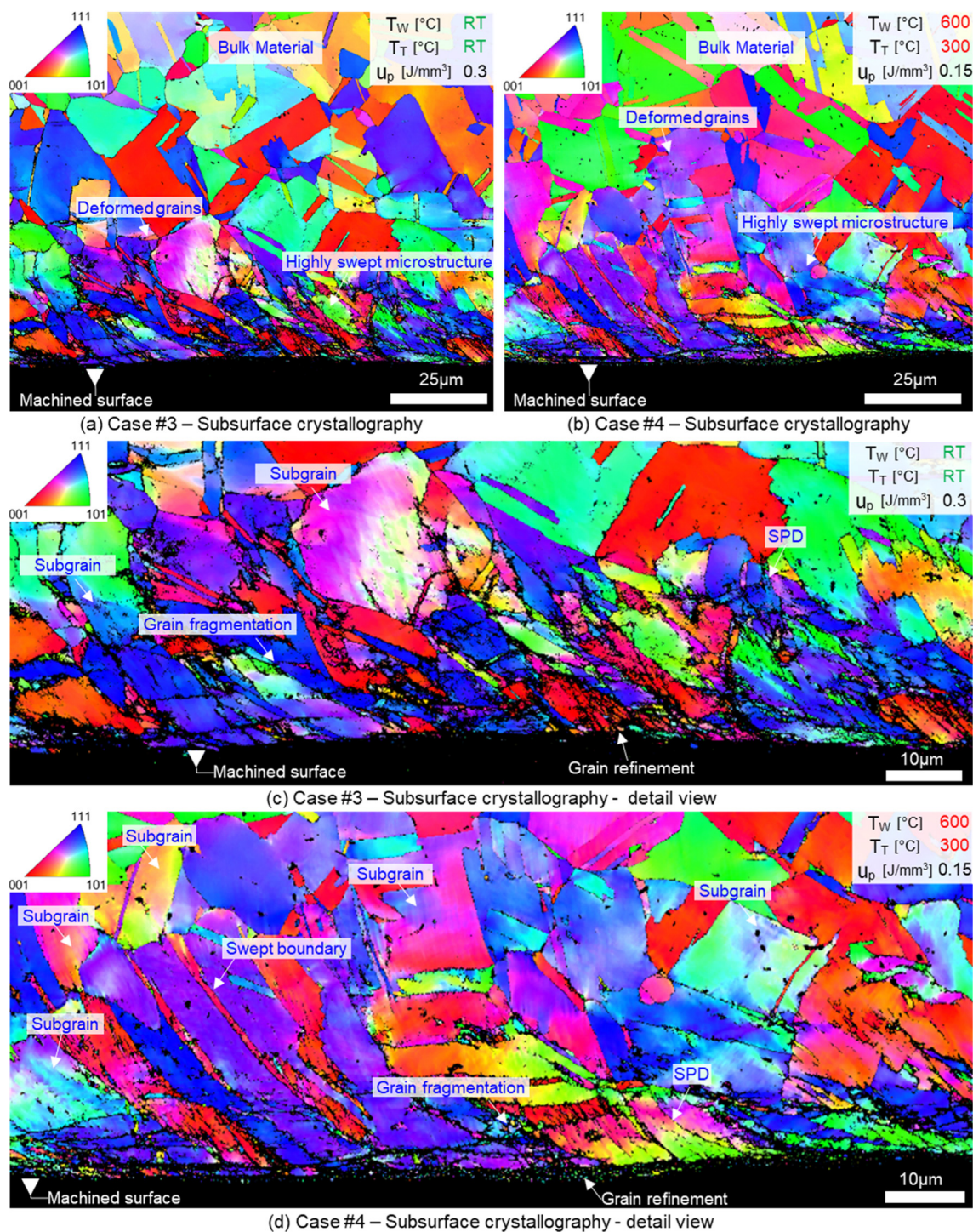


**Fig. 14.** Electron backscatter diffraction (EBSD) analysis of subsurface change in crystallographic orientation under high mechanical effects. (a) Microstructural deformation under lower thermal effects and (b) near-surface detail. (c) Microstructural deformation under higher thermal effects and (d) near-surface detail. Despite the decrease in cutting energy at higher temperature, lattice distortion propagates at high subsurface depths in both low and high temperature regimes.

From a thermo-mechanical perspective, the onset of this phenomenon at higher cutting temperature is controlled by the reciprocal influence between thermal softening and shear localisation. On one hand, increased material softening at higher cutting temperatures promotes shear localisation in PSZ. In fact, the plastic flow of softened material in PSZ at higher temperatures acts as a “weak-link”, offering minimal resistance to further strain, which makes it a preferential deformation site and leads to the observed

shear localisation. On the other hand, the increased shear localisation in PSZ results in intensive heat generation, which in turns promotes further thermal softening effects. In fact, in Ni-base superalloys this is additionally emphasised by their low thermal diffusivity, which leads to heat localisation and consequent softening effects in the shear bands. From a microstructural perspective, this results in a heterogeneous crystalline texture, with larger and deformed grains populating the central regions of the chip seg-

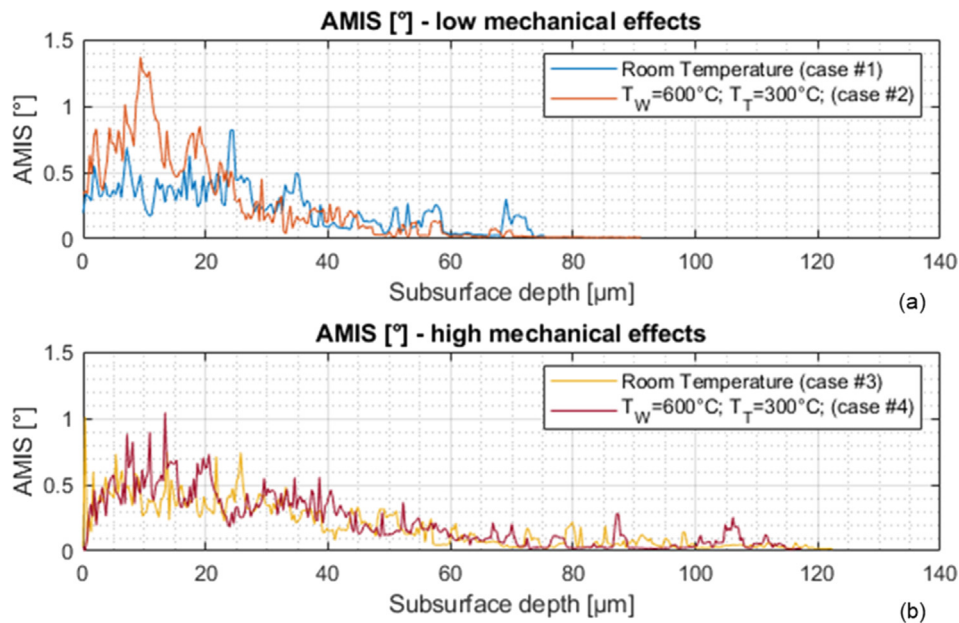


**Fig. 15.** Average intra-grain misorientation (AMIS) profiles for workpiece subsurfaces machined under different combinations of thermal and mechanical effects. (a) Subsurface AMIS profiles under low mechanical effects, showing that higher thermal regimes produced high AMIS values within similar subsurface depths despite the decrease in cutting forces and energy. (b) Subsurface AMIS profiles under high mechanical effects, showing that higher thermal regimes produced high AMIS values within similar subsurface depths despite the decrease in cutting forces and energy.

ments, showing high intra-granular misorientation levels (Fig. 17d) as a result of the dislocation network induced by the plastic deformation process.

On the contrary, the grain-refinement region in correspondence of the chip shear bands presents a much lower intra-granular misorientation. In fact, with the higher temperatures and increased strain localisation, the shear-induced dislocation network in PSZ resolved in the formation of a multitude new boundaries, thus generating a nanocrystalline grain structure. Nevertheless, although higher temperatures led to a greater degree of microstructural reconfiguration, this only involved a narrow portion of the chip volume (Fig. 17c-d). As a result, this deformation mechanism required overall less energy and resulted in lower cutting forces, in contrast with the less intensive but more distributed deformation observed at lower temperatures (Fig. 17a-b).

Thus, comparison of the low speed experiments ( $V_c = 50$  m/min,  $\alpha = 0^\circ$ ,  $r = 25$  μm) at low (RT) and high temperature ( $T_w = 600$  °C,  $T_T = 300$  °C) showed how the onset of chip serration with occurrence of shear banding and nanocrystalline grain refinement can be driven solely by an increase in the thermal boundary conditions. From this point, what would be the influence of an increase also in the mechanical effects?

An even more remarkable microstructural evolution is observed when cutting at *high-speed/high-temperature* ( $V_c = 140$  m/min,  $\alpha = -10^\circ$ ,  $r = 50$  μm,  $T_w = 600$  °C,  $T_T = 300$  °C), as shown in Fig. 18. Extreme levels of chip serration (Fig. 18a) are microstructurally achieved through a combination of nanoscale recrystallisation in the shear band regions (Fig. 18b), together with large amounts of microstructural deformation (Fig. 18c) propagating from the shear localisation sites towards the inner regions of the chip segments. In fact, such large crystals deforming at the confluence of consecutive chip segments (Fig. 18d) present high levels of intra-granular misorientation (Fig. 18e).

In this way, the increased lattice rotation leading to high dislocation densities ultimately degenerates into recrystallisation when reaching the narrow primary shear banding region. Thus, this indicates that the grain refinement mechanism during chip

formation is in the first place controlled by accumulation of plastic strain, which generates significant lattice misorientation associated with high-density dislocation networks, and further promoted by higher thermal regimes, which facilitate strain localisation effects due to thermal softening, and additionally provide thermal energy for the formation of new grain boundaries. Finally, it is observed how the increase in mechanical effects at high temperature further induced the formation of an additional recrystallisation layer in correspondence of the secondary shear zone (SSZ), where the chip back surface frictionally slides along the insert's rake face (Fig. 18d). Similarly to the shear banding region, lower intra-granular misorientation is observed also within the SSZ as a result of the nanoscale recrystallisation process (Fig. 18e).

This sub-microscale phenomenon can be further related to the macroscale change in energy partition discussed in Section 4.1, where it was noted that the frictional energy dissipated at the tool-chip interface became predominant under higher mechanical effects. Such frictional energy is in fact dissipated in the form of heat in SSZ and employed by the chip lattice to rearrange generating continuous grain refinement layer on its back surface.

## 5. Conclusions

Understanding the small-scale mechanisms of microstructural reconfiguration during chip formation is essential to control the surface integrity of machined parts, especially when processing high-performance materials for safety-critical applications. In fact, heat generation due to the tool-workpiece mechanical interaction can influence the thermal conditions under which plastic deformation take place. However, within conventional cutting scenarios it results difficult to identify in which way the onset of microstructural reconfiguration and shear localisation is thermally or mechanically activated, primarily because increasing cutting temperatures are also associated to a more aggressive tool-workpiece mechanical interaction.

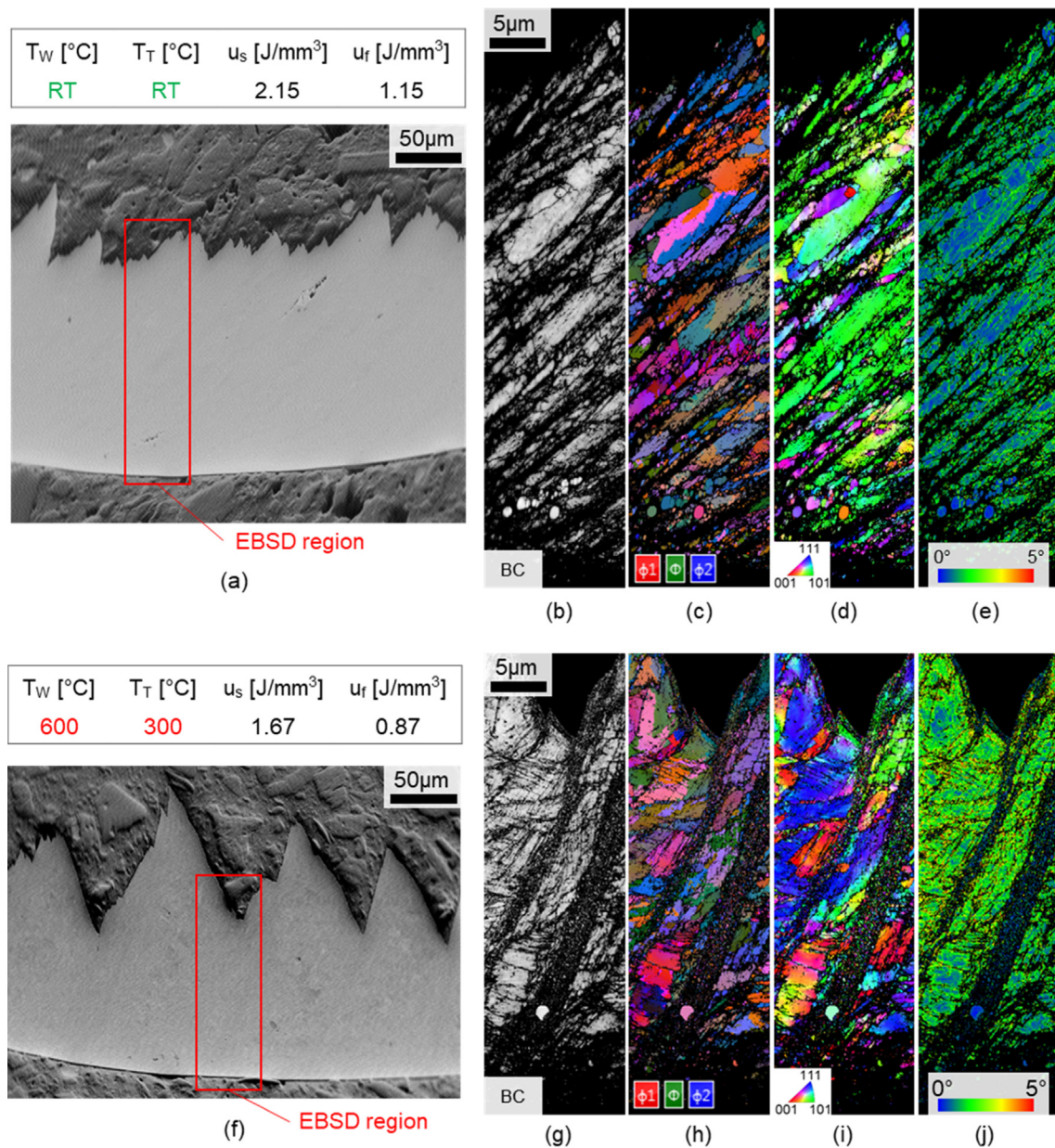


**Fig. 16.** Temperature-dependent microstructural reconfiguration governing chip formation under low mechanical effects. An increase in shear localisation leading to recrystallisation is promoted by higher temperatures under same mechanical effects. (a) Moderately serrated chip micrograph produced under low mechanical effects and low thermal effects - case #1. (b) Band contrast (BC) map in shear localisation region - case #1. (c) Euler map - case #1. (d) Inverse pole figure (IPF) map - case #1. (e) Intra-grain misorientation map - case #1. (f) Increasingly serrated chip micrograph produced under low mechanical effects but higher thermal effects - case #2. (g) Band contrast (BC) map in shear localisation region - case #2. (h) Euler map - case #2. (i) Inverse pole figure (IPF) map - case #2. (j) Intra-grain misorientation map - case #2.

Thus, to disclose the temperature-dependent effects on shear localisation and grain refinement, the present work has investigated the microstructural evolution induced when cutting a Ni-base superalloy (Alloy 718) under superimposed thermal regimes. Thus, for the first time, the interplay between workpiece microstructural reconfiguration, chip formation mechanism, energy partition and shear localisation has been studied under a controlled set of thermal and mechanical boundary conditions. This has been achieved through the design of a novel experimental setup allowing to in-situ heat-up both the workpiece material and the cutting insert through dedicated PID temperature controllers, together with in-situ monitoring of the cutting process and in-depth material analysis of machining-induced microstructural reconfiguration. In particular:

- Transition from continuous to serrated chip formation with increased shear localisation can be thermally-activated solely by increase in cutting temperatures, which is observed under the same set of cutting parameters producing a relatively low-intensity mechanical interaction ( $V_C = 50$  m/min,  $\alpha = 0^\circ$ ,  $r = 2$  5  $\mu$ m). The EBSD analysis of the chip shear localisation regions revealed two different shear mechanisms at room temperature (RT) and high temperatures (HT). Continuous chip formation at RT involved a relatively homogenous microstructural deformation pattern, with grain elongation more evenly distributed throughout the chip volume and with low amounts of micro-scale grain refinement. On the contrary, a heterogeneous microstructural condition was found under HT chip formation ( $T_W = 600$  °C,  $T_T = 300$  °C), with presence of nanoscale grain

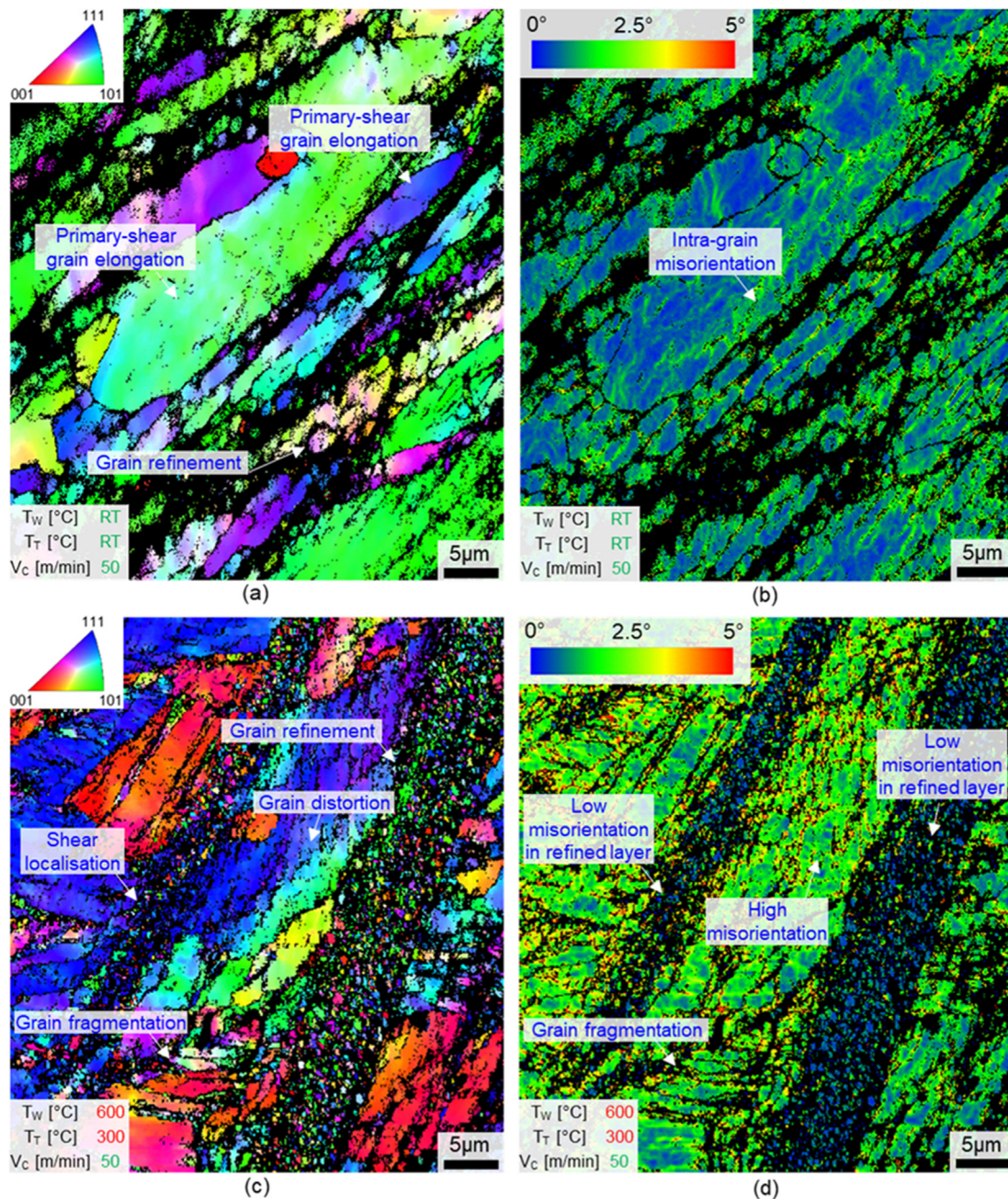


**Fig. 17.** Detail of temperature-dependent chip shear localisation mechanism and microstructural evolution (a) Low-temperature grain elongation and (b) intra-grain misorientation map. (c) High-temperature grain refinement with (b) lower intra-grain misorientation in the recrystallised region.

refinement in narrow shear localisation regions at the boundary between large-grained chip segments. Further, this showed that promotion of nanoscale recrystallisation and increased chip serration at higher temperatures is controlled by the reciprocal interplay between thermal softening and shear localisation in the primary deformation zone.

- An increase in mechanical interaction ( $V_c = 140$  m/min,  $\alpha = -10^\circ$ ,  $r = 50$  μm) at high temperature ( $T_w = 600$  °C,  $T_r = 300$  °C) induced large plastic deformation within the chip segments, with the formation two nanoscale grain refinement layers, a first one in correspondence of the primary shear zone, and an additional one continuously propagating along the chip back

surface, i.e. in correspondence of the secondary shear zone. This microstructural phenomenon is associated to the macroscopically observed a change in energy partition at the tool-workpiece interface, with most of the cutting energy being dissipated as a result of the frictional interaction between the chip and the cutting insert's rake face.

- Larger values of intra-granular misorientation are observed in all the larger-grained regions in each of the machined chips, both at RT and HT, while it was minimal within the nanocrystalline layers. This indicates that grain refinement is mechanically preceded by strain-induced intra-granular dislocation networks, whose degeneration into recrystallisation is assisted

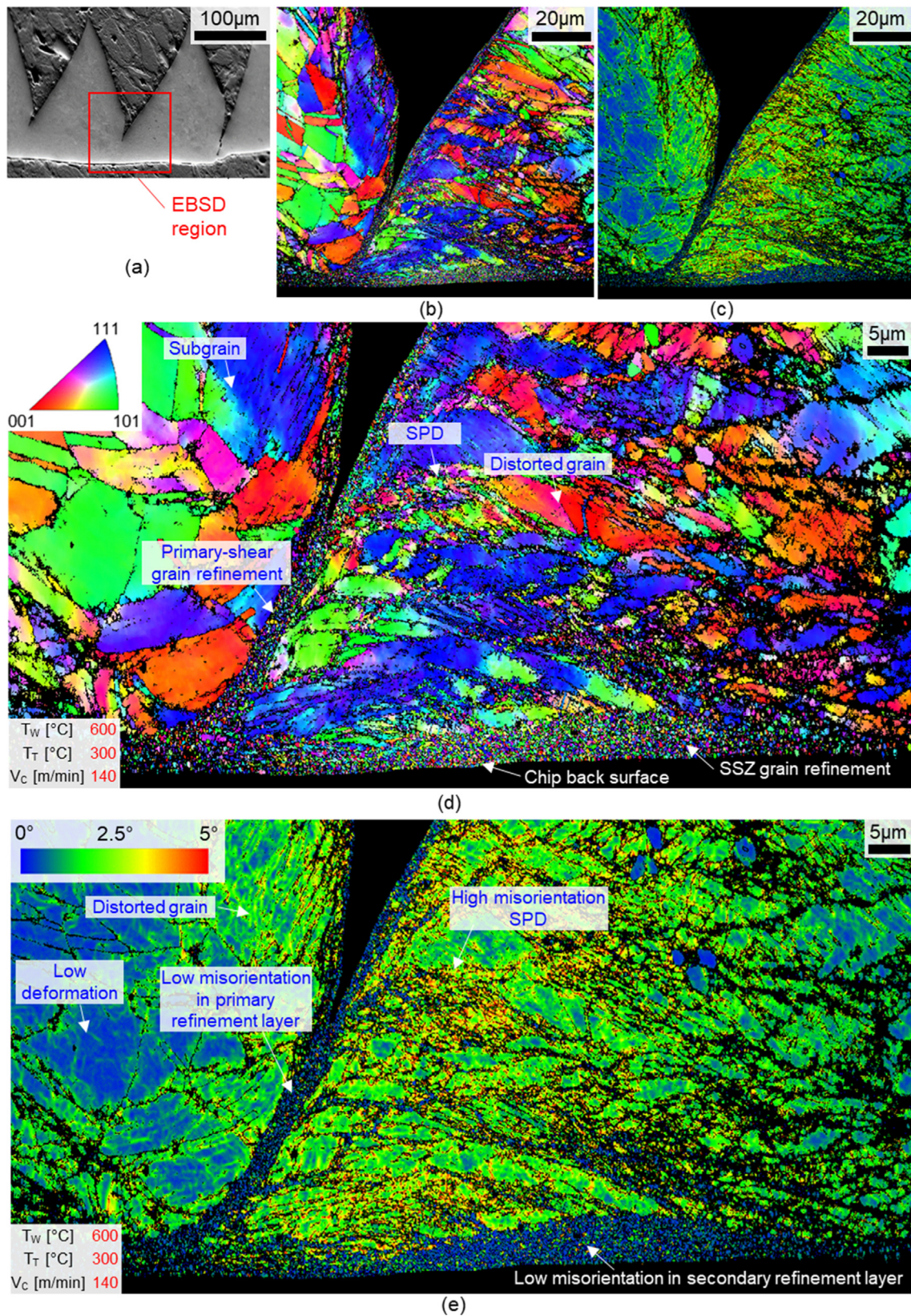


**Fig. 18.** High-temperature chip shear localisation mechanism and microstructural evolution under high mechanical effects (a) Highly-serrated chip morphology. (b) IPF crystallographic map. (c) Misorientation map. (d) Detail of IPF map in shear localisation region and (e) detail view of misorientation map in shear localisation region.

by higher temperature conditions as HT conditions promote strain localisation and additionally provide thermal energy for recrystallisation. Hence the observed transition between machining-induced microstructural reconfiguration regime and chip formation mechanisms is mechanically driven through strain accumulation and further promoted by higher thermal fields.

- From a macroscopic perspective, the thermally-driven increase in chip serration resulted in lower cutting forces, shear energy and friction energy, decreasing in the range of  $\sim 25\text{--}30\%$  at higher temperature ( $T_W = 600\text{ }^\circ\text{C}$ ,  $T_T = 300\text{ }^\circ\text{C}$ ) compared to each respective room temperature condition, both under low ( $V_C = 50\text{ m/min}$ ,  $\alpha = 0^\circ$ ,  $r = 25\text{ }\mu\text{m}$ ) and high ( $V_C = 140\text{ m/min}$ ,  $\alpha = -10^\circ$ ,  $r = 50\text{ }\mu\text{m}$ ) mechanical effects. This behaviour is microscopically controlled by the fact that under lower thermal fields the chip plastic deformation is more distributed and hence more uniformly involved the entire chip volume, while HT primary shear is instead more intensive but also much more localised. Therefore, onset of shear localisation is more energetically-favourable as the material removal is achieved by deforming the chip mostly along a very narrow and softened band of material.
- To this point, the levels of machining-induced surface integrity was only associated to the amount of energy required to perform chip formation. However, this study proved how the relationship between cutting energy and microstructural deformation is temperature-dependent, as it is affected by the constitutive behaviour of the workpiece material. In fact, despite the much lower energy consumption under HT conditions, the thickness of the microstructurally-deformed workpiece layers presented similar or even greater values. In particular, the cutting energy decrease at higher temperatures corresponded to an increase in deformation layer thickness as a result of a non-negligible thermal softening in the HT range with respect to RT. Therefore, this highlights the need for future studies to take in strong consideration the role of temperature-dependent effects when further exploring the link between deformation energy and microstructural surface integrity.

Although this study focused on the deformation mechanism of a representative Ni-base superalloy (Alloy 718), the present approach could be directly employed to understand the temperature-dependent response of many more material systems, such as Ti alloys, steels, metal or ceramic matrix composites, ceramics, and more. Moreover, broader application of the experience linking microstructural evolution and thermal regime may also provide key insights to the understanding of other thermo-mechanical processes such as metal forming, hot-rolling, friction welding, supporting the effective realisation of next-generation materials processing approaches based on an in-depth understanding and awareness of the thermo-mechanically-induced mechanisms of workpiece microstructural reconfiguration.

### CRedit authorship contribution statement

**Andrea la Monaca:** Conceptualization, Methodology, Investigation, Formal analysis, Visualization, Data curation, Writing – original draft, Writing – review & editing. **Dragos A. Axinte:** Conceptualization, Methodology, Formal analysis, Visualization, Supervision, Writing – review & editing. **Zhirong Liao:** Conceptualization, Formal analysis, Resources, Supervision, Writing – review & editing. **Rachid M'Saoubi:** Formal analysis, Resources, Supervision, Writing – review & editing. **Mark C. Hardy:** Formal analysis, Resources, Supervision, Writing – review & editing.

### Data Availability.

The raw/processed data required to reproduce these findings cannot be shared at this time as the data also forms part of an ongoing study.

### Declaration of Competing Interest

The authors declare that they have no known competing financial interests or personal relationships that could have appeared to influence the work reported in this paper.

### Acknowledgment

The authors would like to acknowledge Rolls-Royce plc and Seco Tools AB for permission to publish this work and provision of financial support. This study was further supported by the EPSRC through the NanoPrime initiative (EPSRC Reference: EP/R025282/1). The Nanoscale and Microscale Research Centre (nmRC) at the University of Nottingham is also acknowledged for providing access to their facilities. The authors would also like to express their gratitude to Mr Stephen Hall and Mr Daniel Foreman from the University of Nottingham for their technical support within the manufacture of the parts for the pendulum-based experimental set-up.

### References

- [1] Z. Liao, A. la Monaca, J. Murray, A. Speidel, D. Ushmaev, A. Clare, D. Axinte, R. M'Saoubi, Surface integrity in metal machining - Part I: Fundamentals of surface characteristics and formation mechanisms, *Int. J. Mach. Tools Manuf.* 162 (2021), <https://doi.org/10.1016/j.ijmactools.2020.103687> 103687.
- [2] K. Winter, Z. Liao, R. Ramanathan, D. Axinte, G. Vakil, C. Gerada, How non-conventional machining affects the surface integrity and magnetic properties of non-oriented electrical steel, *Mater. Des.* 210 (2021), <https://doi.org/10.1016/j.matdes.2021.110051> 110051.
- [3] M.C. Shaw, *Metal cutting principles* (Second edition), Oxford University Press, 2005. <https://doi.org/10.1037/023990>.
- [4] S. Imbrogno, S. Rinaldi, D. Umbrello, L. Filice, R. Franchi, A. Del Prete, A physically based constitutive model for predicting the surface integrity in machining of Waspaloy, *Mater. Des.* 152 (2018) 140–155.
- [5] A. Thakur, S. Gangopadhyay, State-of-the-art in surface integrity in machining of nickel-based super alloys, *Int. J. Mach. Tools Manuf.* 100 (2016) 25–54, <https://doi.org/10.1016/j.ijmactools.2015.10.001>.
- [6] A. la Monaca, Z. Liao, D. Axinte, A digital approach to automatically assess the machining-induced microstructural surface integrity, *J. Mater. Process. Technol.* 282 (2020), <https://doi.org/10.1016/j.jmatprotec.2020.116703> 116703.
- [7] T. Conolly, M.J. Starink, P.A.S. Reed, Effect of broaching on high-temperature fatigue behavior in notched specimens of INCONEL 718, *Metal and Mat Trans A* 35 (3) (2004) 771–783.
- [8] A. la Monaca, J.W. Murray, Z. Liao, A. Speidel, J.A. Robles-Linares, D.A. Axinte, M.C. Hardy, A.T. Clare, Surface integrity in metal machining - Part II: Functional performance, *Int. J. Mach. Tools Manuf.* 164 (2021), <https://doi.org/10.1016/j.ijmactools.2021.103718> 103718.
- [9] A.M. Wusatowska-Sarneck, B. Dubiel, A. Czyska-Filemonowicz, P.R. Bhowal, N. Ben Salah, J.E. Klemberg-Sapieha, Microstructural characterization of the white etching layer in nickel-based superalloy, *Metall. Mater. Trans. A Phys. Metall. Mater. Sci.* 42 (2011) 3813–3825, <https://doi.org/10.1007/s11661-011-0779-8>.
- [10] J. Telesman, T.P. Gabb, P.T. Kantzos, L.J. Ghosn, Effect of broaching machining parameters, residual stresses and cold work on fatigue life of Ni-based turbine disk P/M alloy at 650 °C, *Int. J. Fatigue* 150 (2022), <https://doi.org/10.1016/j.ijfatigue.2021.106328> 106328.
- [11] M. Brown, D. Pieris, D. Wright, P. Crawforth, R. M'Saoubi, J. McGourlay, A. Mantle, R. Patel, R.J. Smith, H. Ghadbeigi, Non-destructive detection of machining-induced white layers through grain size and crystallographic texture-sensitive methods, *Mater. Des.* 200 (2021), <https://doi.org/10.1016/j.matdes.2021.109472> 109472.
- [12] Z. Ren, Z. Fang, T. Kizaki, Y. Feng, T. Nagata, Y. Komatsu, N. Sugita, Understanding local cutting features affecting surface integrity of gear flank in gear skiving, *Int. J. Mach. Tools Manuf.* 172 (2022), <https://doi.org/10.1016/j.ijmactools.2021.103818> 103818.
- [13] Y. Zhang, R. Kang, Z. Dong, Q. Wang, X. Zhu, R. Xu, D. Guo, Microstructural evolution of soft magnetic 49Fe-49Co-2V alloy induced by drilling, *Mater. Des.* 189 (2020), <https://doi.org/10.1016/j.matdes.2020.108501> 108501.

- [14] N.A. Abukhshim, P.T. Mativenga, M.A. Sheikh, Heat generation and temperature prediction in metal cutting: A review and implications for high speed machining, *Int. J. Mach. Tools Manuf.* 46 (7-8) (2006) 782–800.
- [15] H. Jiang, C. Wang, Z. Ren, Y. Yi, L. He, X. Zhao, Influence of cutting velocity on gradient microstructure of machined surface during turning of high-strength alloy steel, *Mater. Sci. Eng. A* 819 (2021), <https://doi.org/10.1016/j.msea.2021.141354> 141354.
- [16] B. Medina-Clavijo, M. Saez-de-Buruaga, C. Motz, D. Soler, A. Chuvilin, P.J. Arrazola, Microstructural aspects of the transition between two regimes in orthogonal cutting of AISI 1045 steel, *J. Mater. Process. Technol.* 260 (2018) 87–96, <https://doi.org/10.1016/j.jmatprotec.2018.05.016>.
- [17] S.B. Hosseini, U. Klement, Y. Yao, K. Rytberg, Formation mechanisms of white layers induced by hard turning of AISI 52100 steel, *Acta Mater.* 89 (2015) 258–267, <https://doi.org/10.1016/j.actamat.2015.01.075>.
- [18] Z. Liao, M. Polyakov, O.G. Diaz, D. Axinte, G. Mohanty, X. Maeder, J. Michler, M. Hardy, Grain refinement mechanism of nickel-based superalloy by severe plastic deformation - Mechanical machining case, *Acta Mater.* 180 (2019) 2–14, <https://doi.org/10.1016/j.actamat.2019.08.059>.
- [19] B. Wang, Z. Liu, Evaluation on fracture locus of serrated chip generation with stress triaxiality in high speed machining of Ti6Al4V, *Mater. Des.* 98 (2016) 68–78, <https://doi.org/10.1016/j.matdes.2016.03.012>.
- [20] H. Liu, J. Zhang, B. Xu, X. Xu, W. Zhao, Prediction of microstructure gradient distribution in machined surface induced by high speed machining through a coupled FE and CA approach, *Mater. Des.* 196 (2020), <https://doi.org/10.1016/j.matdes.2020.109133> 109133.
- [21] Q. Liu, Z. Liao, D. Axinte, Temperature effect on the material removal mechanism of soft-brittle crystals at nano/micron scale, *Int. J. Mach. Tools Manuf.* 159 (2020), <https://doi.org/10.1016/j.ijmactools.2020.103620> 103620.
- [22] M. Harzallah, T. Pottier, R. Gilblas, Y. Landon, M. Mousseigne, J. Senatore, Thermomechanical coupling investigation in Ti-6Al-4V orthogonal cutting: Experimental and numerical confrontation, *Int. J. Mech. Sci.* 169 (2020), <https://doi.org/10.1016/j.ijmecsci.2019.105322> 105322.
- [23] A. la Monaca, D.A. Axinte, Z. Liao, R. M'Saoubi, M.C. Hardy, Towards understanding the thermal history of microstructural surface deformation when cutting a next generation powder metallurgy nickel-base superalloy, *Int. J. Mach. Tools Manuf.* 168 (2021), <https://doi.org/10.1016/j.ijmactools.2021.103765> 103765.
- [24] J.D. Pérez-Ruiz, L.N.L. de Lacalle, G. Urbikain, O. Pereira, S. Martínez, J. Bris, On the relationship between cutting forces and anisotropy features in the milling of LPBF Inconel 718 for near net shape parts, *Int. J. Mach. Tools Manuf.* 170 (2021), <https://doi.org/10.1016/j.ijmactools.2021.103801> 103801.
- [25] A. Malakizadi, T. Hajali, F. Schulz, S. Cedergren, J. Ålgårdh, R. M'Saoubi, E. Hryha, P. Krajnik, The role of microstructural characteristics of additively manufactured Alloy 718 on tool wear in machining, *Int. J. Mach. Tools Manuf.* 171 (2021), <https://doi.org/10.1016/j.ijmactools.2021.103814> 103814.
- [26] A.W. Nemetz, W. Daves, T. Klünsner, W. Ecker, J. Schäfer, C. Czettl, T. Antretter, Cyclic heat-up and damage-relevant substrate plastification of single- and bilayer coated milling inserts evaluated numerically, *Surf. Coatings Technol.* 360 (2019) 39–49, <https://doi.org/10.1016/j.surfcoat.2019.01.008>.
- [27] M. Zhang, D. Zhang, D. Geng, J. Liu, Z. Shao, X. Jiang, Surface and sub-surface analysis of rotary ultrasonic elliptical end milling of Ti-6Al-4V, *Mater. Des.* 191 (2020), <https://doi.org/10.1016/j.matdes.2020.108658> 108658.
- [28] M. Cuesta, P. Aristimuño, A. Garay, P.J. Arrazola, Heat transferred to the workpiece based on temperature measurements by IR technique in dry and lubricated drilling of Inconel 718, *Appl. Therm. Eng.* 104 (2016) 309–318, <https://doi.org/10.1016/j.applthermaleng.2016.05.040>.
- [29] D. Xu, Z. Liao, D. Axinte, J.A. Sarasua, R. M'Saoubi, A. Wretland, Investigation of surface integrity in laser-assisted machining of nickel based superalloy, *Mater. Des.* 194 (2020), <https://doi.org/10.1016/j.matdes.2020.108851> 108851.
- [30] S. Joshi, A. Tewari, S. Joshi, Influence of Preheating on Chip Segmentation and Microstructure in Orthogonal Machining of Ti6Al4V, *J. Manuf. Sci. Eng.* 135 (2013) 1–11, <https://doi.org/10.1115/1.4025741>.
- [31] D. Zhang, X.-M. Zhang, G.-C. Nie, Z.-Y. Yang, H. Ding, Characterization of material strain and thermal softening effects in the cutting process, *Int. J. Mach. Tools Manuf.* 160 (2021), <https://doi.org/10.1016/j.ijmactools.2020.103672> 103672.
- [32] D. Ambrosio, A. Tongne, V. Wagner, G. Dessein, O. Cahuc, A new damage evolution criterion for the coupled Eulerian-Lagrangian approach: Application to three-dimensional numerical simulation of segmented chip formation mechanisms in orthogonal cutting, *J. Manuf. Process.* 73 (2022) 149–163, <https://doi.org/10.1016/j.jmapro.2021.10.062>.
- [33] M.P. Sealy, Z.Y. Liu, Y.B. Guo, Z.Q. Liu, Energy based process signature for surface integrity in hard milling, *J. Mater. Process. Technol.* 238 (2016) 284–289, <https://doi.org/10.1016/j.jmatprotec.2016.07.038>.
- [34] E. Brinksmeier, F. Klocke, D.A. Lucca, J. Söller, D. Meyer, Process Signatures – a new approach to solve the inverse surface integrity problem in machining processes, *Procedia CIRP* 13 (2014) 429–434, <https://doi.org/10.1016/j.procir.2014.04.073>.
- [35] D. Xu, Z. Liao, D. Axinte, M. Hardy, R. M'Saoubi, A quick method for evaluating the thresholds of workpiece surface damage in machining, *CIRP Ann.* 68 (2019) 61–64, <https://doi.org/10.1016/j.cirp.2019.03.015>.
- [36] E. Budak, E. Ozlu, H. Bakioglu, Z. Barzegar, Thermo-mechanical modeling of the third deformation zone in machining for prediction of cutting forces, *CIRP Ann. - Manuf. Technol.* 65 (2016) 121–124, <https://doi.org/10.1016/j.cirp.2016.04.110>.
- [37] D. Xu, Z. Liao, D. Axinte, M. Hardy, A novel method to continuously map the surface integrity and cutting mechanism transition in various cutting conditions, *Int. J. Mach. Tools Manuf.* 151 (2020), <https://doi.org/10.1016/j.ijmactools.2020.103529> 103529.
- [38] E. Hosseini, V.A. Popovich, A review of mechanical properties of additively manufactured Inconel 718, *Addit. Manuf.* 30 (2019), <https://doi.org/10.1016/j.addma.2019.100877> 100877.
- [39] C. Herbert, D.A. Axinte, M. Hardy, P. Withers, Influence of surface anomalies following hole making operations on the fatigue performance for a nickel-based superalloy, *J. Manuf. Sci. Eng. Trans. ASME* 136 (2014) 1–9, <https://doi.org/10.1115/1.4027619>.
- [40] Z. Liao, D. Axinte, M. Mieszala, R. M'Saoubi, J. Michler, M. Hardy, On the influence of gamma prime upon machining of advanced nickel based superalloy, *CIRP Ann.* 67 (2018) 109–112, <https://doi.org/10.1016/j.cirp.2018.03.021>.
- [41] L.N. Brewer, M.A. Othon, Y. Gao, B.T. Hazel, W.H. Buttrill, Z. Zhong, Comparison of diffraction methods for measurement of surface damage in superalloys, *J. Mater. Res.* 21 (2006) 1775–1781, <https://doi.org/10.1557/jmr.2006.0199>.
- [42] T. Childs, Adiabatic Shearing in Metal Machining, in: *CIRP Encycl. Prod. Eng.*, Springer Berlin Heidelberg, Berlin, Heidelberg, 2014: pp. 27–33. [https://doi.org/10.1007/978-3-642-20617-7\\_6392](https://doi.org/10.1007/978-3-642-20617-7_6392).
- [43] D. Sagapuram, K. Viswanathan, K.P. Trumble, S. Chandrasekar, A common mechanism for evolution of single shear bands in large-strain deformation of metals, *Philos. Mag.* 98 (2018) 3267–3299, <https://doi.org/10.1080/14786435.2018.1524586>.